ginal case in which the equality sign holds in Eq. (3.41).

[11]An explanation of why a less stringent set of necessary conditions was previously obtained is given in Ref. 3(e), where the more stringent set is proved.

[12]The assertion in the treatise by Blatt and Weisskopf [Ref. 2, p. 150, after Eq. (4.40)] is actually incorrect on two accounts. The Wigner proof (Ref. 1) does not consider the most general mixture of exchange forces, and therefore it does not purport to provide any information for that case. Further, the set of conditions given is *not* sufficient for saturation.

[13]Here we use the assumption that the potential functions are finite (nondivergent) at zero separation.

[14]The discussion given in preceding papers (Ref. 6) can be extended without change to our case.

[15]Even if all the other potentials were characterized by hard cores, in this case there would be no saturation (unless all the potentials are everywhere attractive, in which case of course there is no binding whatsoever). This conclusion is implied by Theorem 1 of Ref. 3(a) [see also Ref. 3(e)].

[16]The possibility of combining the different conditions follows trivially from their proofs.

[17]Even if these classes are enlarged according to the prescription mentioned in the last part of the statement of the Theorem.

[18]This is of course by no means a realistic potential. In this connection, however, the possible usefulness of testing separate pieces of the nuclear force as regards their compatibility with saturation should be reemphasized [see Sec. 1 of this paper, and Refs. 3(c)–3(e)].

[19]Many potentials belong to this class, for instance the sum of two Yukawa or of two Gaussian functions (if the longer-range term is attractive).

[20]Except for their ordering, which in Eq. (3.42) has been chosen to correspond to the "traditional" one (Ref. 2).

PHYSICAL REVIEW C VOLUME 5, NUMBER 5 MAY 1972

Scattering of Neutrons by Carbon from 3 to 7 MeV*

W. Galati,†‡ J. D. Brandenberger, and J. L. Weil
Department of Physics, University of Kentucky, Lexington, Kentucky 40506
(Received 25 June 1971)

Angular distributions of neutrons elastically scattered from natural carbon have been measured at 32 neutron energies between 3 and 7 MeV with energy spreads ranging from 37 to 165 keV. The angular distributions of neutrons inelastically scattered from ^{12}C have also been measured at the nine highest neutron energies. A phase-shift analysis of the elastic scattering cross sections yields the following spin and parity assignments for the excited states of ^{13}C (E_x,J): 8.3 MeV, $\frac{3}{2}^+$; 8.88 MeV, $\frac{1}{2}^-$; 9.50 MeV, $(\frac{1}{2}, \frac{3}{2})^-$; 9.90 MeV, $\frac{3}{2}^-$; 10.75 MeV, $\frac{7}{2}^-$; 11.00 MeV, $(\frac{1}{2}^+)$. Neutron polarizations calculated from the extracted phase shifts agree fairly well with most of the available polarization measurements. A polarization contour map is given showing that carbon may be useful as a polarization analyzer between 4.5 and 7 MeV.

I. INTRODUCTION

Measurements at many laboratories[1-5] of the $^{12}C + n$ total cross section in the energy range from 3.0 to 7.0 MeV reveal resonances at neutron bombarding energies of 3.5, 4.23, 4.93, 5.37, 6.29, and 6.6 MeV. These resonances correspond to excited states of ^{13}C with excitation energies E_x of 8.3, 8.86, 9.50, 9.90, 10.75, and 11.0 MeV, respectively. Differential cross sections for the elastic scattering of neutrons from ^{12}C have been measured and analyzed in the energy range from 2.4 to 3.65 MeV by Meier, Scherrer, and Trumpy (MST)[6]; from 1.5 to 4.1 MeV by Wills *et al.*[7]; and from 3.0 to 4.7 MeV by Lister and Sayres.[8]

Since the ground-state spin of ^{12}C is 0^+, the channel spin has only the value $S = \frac{1}{2}$, which simplifies the problem of performing the phase-shift analysis of differential cross sections. Analyses of these cross sections by the above three groups[6-8] show reasonable agreement with each other in the regions of overlap of bombarding energy and give a relatively consistent set of phase shifts for the whole energy range of the measurements. It is found from these analyses that the very broad level at $E_x = 8.3$ MeV in ^{13}C has a spin and parity of $\frac{3}{2}^+$. An assignment of $\frac{1}{2}^-$ for the level at 8.9 MeV is given by Lister and Sayres.[8] From the total-cross-section measurements of Fossan *et al.*,[1] spin limitations have been placed on the excited states between 9- and 11-MeV excitation as follows: $E_x = 9.50$ MeV, $J \geq \frac{1}{2}$; $E_x = 9.90$ MeV, $J \geq \frac{3}{2}$; $E_x = 10.75$ MeV, $J \geq \frac{7}{2}$.

Very recently Perey and Kinney[9] have reported $^{12}C(n, n)^{12}C$ angular distributions measured at eight bombarding energies between 4.6 and 7.0 MeV. Angular distributions of $^{12}C(n, n)^{12}C$ have also been measured with good energy resolution

at single bombarding energies in the energy range $E_n = 4-7$ MeV by Walt and Beyster,[10] Hill,[11] and Braley and Cook,[12] and with poor energy resolution by Beyster, Walt, and Salmi.[13] There are also some unpublished measurements at these energies.[14] None of these measurements have been subjected to phase-shift analysis.

In the present work, 32 elastic and 9 inelastic angular distributions in the energy range from 3.0 to 6.9 MeV have been measured, and a phase-shift analysis of the elastic data has been carried out. Complex phase shifts were used above a neutron bombarding energy of 4.8 MeV, the threshold for inelastic scattering. Level parameters derived from the analysis are presented, as well as polarizations calculated from the derived phase shifts. The work reported here confirms earlier results below 4.5 MeV and gives J^π assignments for several resonances between 4.5 and 7 MeV.

II. EXPERIMENT

A. Apparatus

Time-of-flight techniques were used to collect data for the neutron cross sections.[15] Neutrons with energies between 3.0 and 5.5 MeV were obtained from the T$(p, n)^3$He reaction, and between 5.5 and 7.0 MeV from the D$(d, n)^3$He reaction. Gas targets were used for both reactions. Target assemblies for both tritium and deuterium consisted of a tantalum-lined gas cell 3.0 cm long by 0.9 cm in diameter with a thin entrance foil. For measurements where the resulting neutron energy spread could be tolerated, the gas cells were operated at 1 atm pressure and the foil was 0.000 76-cm-thick molybdenum. For cases requiring incident neutrons with less energy spread, gas pressures down to 0.3 atm and foils as thin as 0.000 13 cm nickel were used. Terminal-pulsed proton and deuteron beams were obtained from the University of Kentucky HVEC model CN Van de Graaff accelerator. For most of the data taken at neutron energies above 5.5 MeV, a post-acceleration Mobley bunching system was used which gave a pulse duration of less than 1 nsec.[15] The improved signal-to-background ratio due to the bunching helped to overcome the increase in background at the higher neutron energies.

The neutron detector consisted of an organic liquid scintillator 10 cm in diameter by 5 cm thick, optically connected by a silicon fluid to an Amperex 58AVP photomultiplier tube. A fast-timing signal, a linear signal, and a pulse-shape-discrimination (PSD) signal were taken from the neutron detector. The PSD circuit was based on the method of Batchelor.[16] Timing was done by a fast-electronics system made up of standard modules. The signal from the time-to-amplitude converter was fed to a multichannel analyzer which recorded the time spectra. The analyzer was gated by pulses generated by a coincidence between the linear and PSD signals of the neutron detector. With this arrangement, the detector had a threshold of 0.5-MeV neutron energy with a γ-ray rejection of better than 90%.

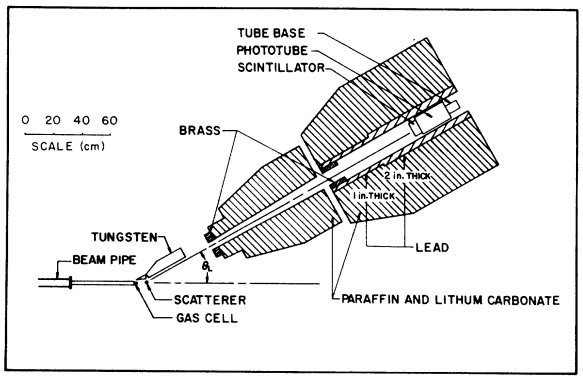

FIG. 1. Apparatus used in $^{12}C + n$ experiment including neutron source, scattering sample, detector shielding, and neutron detector.

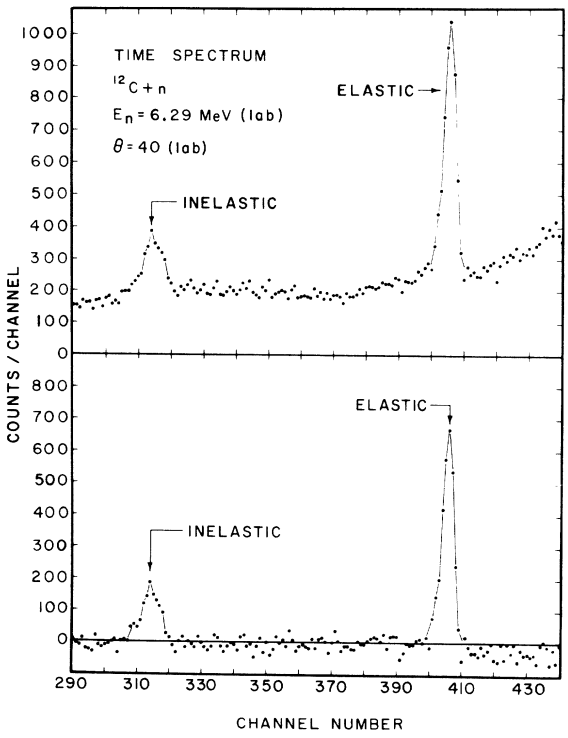

FIG. 2. Time spectrum of 6.29-MeV neutrons scattered from carbon, both before and after subtraction of the sample-out background. The flight path was 1.7 m and the time calibration was 0.51 nsec/channel.

The neutron detector was placed inside a 1.0-m-diam shield of paraffin, lithium carbonate, and lead (see Fig. 1) which could be rotated from an angle of $\theta_L = -100°$ to $\theta_L = +155°$. The distance between the carbon scatterer and detector was typically 170 cm. A tungsten wedge near the neutron source was adjustable to maximize the neutron attenuation between the source and the detector.

A second neutron time-of-flight detector, situated 1.0 m above the source of neutrons, served to monitor the neutron flux. It consisted of a Dumont 6467 photomultiplier tube and a Pilot B plastic scintillator. Fast-timing output signals were fed into a time-to-amplitude converter whose output went to a single-channel analyzer. The analyzer window was set on the neutron peak in the time spectrum, and a scaler counted the output pulses of the single-channel analyzer, giving a measure of the number of neutrons incident on the scatterer.

B. Experimental Procedure

The carbon scatterer used to measure the differential cross sections was made of reactor-grade graphite obtained from Oak Ridge National Laboratory.[17] It was a cylinder 0.892 cm in diameter by 2.57 cm long, and had a mass of 2.651 g. A thin nylon monofilament thread was used to support the carbon sample 9.0 cm from the center of the gas target cell.

A typical time spectrum taken at a neutron energy of 6.29 MeV with a bunched beam is shown in Fig. 2 before and after background subtraction. Data for the angular distributions were taken at 10° intervals between 20 and 150°, though in some cases the measurements extended to 15 and 155°.

The energy calibration of the charged-particle beam was known to ±0.01 MeV. Narrow resonances in the ^{12}C total cross section at laboratory energies of 4.933 ± 0.003, 5.369 ± 0.003, 6.293 ± 0.003, and 6.56 MeV have widths Γ_{lab} of ≤ 5.5, 28 ± 3, 57 ± 4, and 40 ± 4 keV, respectively.[5] For scattering measurements at energies near these resonances the mean energy of the incident neutrons was always accurately determined relative to the resonance maximum or minimum in the total cross section curve by first performing a transmission measurement using Union Carbide grade AUC high-purity graphite. The field of the analyzing magnet was then increased or decreased a small amount to reach the scattering energy. It was determined that hysteresis did not affect the energy calibration when the magnetic field was reduced by the necessary amounts. Three different transmission sample sizes were used (4.8, 8.0, and 18 cm long) which gave approximately 70, 50, and 20% transmission, respectively. Mean incident neutron energies were determined in this way to ±5 keV with respect to the resonance energies of the total cross section.

To obtain absolute differential cross sections, the number of neutrons scattered at 40° by both carbon and hydrogen were measured and then normalized to the known n-p cross section.[18] For angular distributions taken at all energies except 4.15, 4.25, 4.45, and 4.64 MeV a polyethylene cylinder 0.488 cm in diameter by 2.54 cm high and weighing 0.4415 g was used as the hydrogen scatterer. Approximately 10 000 counts were accumulated at each bombarding energy in the group of neutrons scattered by hydrogen, which was generally well resolved from the group scattered by carbon. For angular distributions at the above four energies and H_2O scattering sample of approximately 2 g was used. A thin-walled plastic vial contained the H_2O.

The relative efficiency of the neutron detector over the energy range of interest was measured 6 times during the course of this experiment, and checked a number of times. On most occasions this was done by measuring the angular distributions at several energies and measuring the 0° excitation functions of the reactions $T(p, n)^3He$ and $D(d, n)^3He$. However, on two occasions the relative efficiency was determined wholly or in part from a measurement of the angular distribution of n-p scattering from polyethylene cylinders of 5 mm diam or less. The efficiency curves obtained by the two methods were quite consistent with each other. A current integrator was used as a monitor for the efficiency calibration. The errors in the efficiency-curve data points were calculated to be 4.5% in the energy region between 2 and 5.8 MeV, and were somewhat larger at lower and higher energies. The effect of this uncertainty on the measured cross sections is discussed in Sec. II D.

C. Data Reduction

The elastic differential cross sections were corrected for dead time in the counting electronics, angular spread, flux attenuation, and multiple scattering. The angular spread was $\leq \pm 5\%$ which led to a correction <1%.

Flux-attenuation corrections were made using the method of Cranberg and Levin.[19] They ranged between 3 and 8% for the scattering yields from carbon and were from 3 to 6% for the n-p scattering normalization points.

The method used for making the multiple-scattering corrections was first developed for neutrons by Blok and Jonker,[20] and has been applied to neutron scattering by Walt and Barschall,[21] MST,[6] Wills *et al.*,[7] and more recently by Reber.[22] In the

TABLE I. Differential cross sections $\sigma(\theta)$ of neutrons elastically scattered from carbon for E_n=3.03–4.15 MeV. The errors are rms absolute errors. The rms relative errors can be determined by unfolding the following systematic errors: E_n=3.03–5.15 MeV, $\Delta\sigma_{sys}$=5%; E_n=5.324–6.00 MeV, $\Delta\sigma_{sys}$=6%; E_n=6.25–6.94 MeV, $\Delta\sigma_{sys}$=7%. The uncertainty in scattering angle is estimated to be ±0.5°. Both θ and $\sigma(\theta)$ are in the center-of-mass system. All cross sections are in mb/sr.

θ° \ E_n / ΔE_n	3.03 MeV 80 keV	3.25 MeV 80 keV	3.46 MeV 80 keV	3.67 MeV 75 keV	3.86 MeV 75 keV	4.075 MeV 75 keV	4.15 MeV 70 keV
16.3	203 ±13	350 ±22	606 ±39	717 ±46	526 ±34	437 ±27	386 ±25
21.6	209 ±13	345 ±21	543 ±35	575 ±36	502 ±32	380 ±23	363 ±23
27.0	184 ±12						332 ±22
32.4	170 ±11	308 ±18	438 ±27	437 ±27	392 ±26	284 ±17	260 ±17
43.1	144 ±9.3	257 ±16	327 ±20	319 ±19	253 ±17	185 ±11	192 ±13
53.7	113 ±7.2	184 ±11	220 ±13	192 ±12	148 ±9.5	108 ±6.6	123 ±7.6
64.2	95.0±6.1	103 ±6.3	110 ±7.1	102 ±6.6	81.2±5.8	70.8±4.3	92.4±6.0
74.5	75.1±4.8	48.7±3.0	42.3±3.7	43.0±3.1	51.5±3.6	57.1±3.5	80.9±5.2
84.7	68.3±4.4	13.1±1.2	8.2±0.8	21.7±2.5	43.6±3.1	59.4±3.6	85.9±5.6
94.8	70.9±4.5	11.3±1.3	5.2±0.9	32.0±2.8	54.9±4.0	71.9±4.4	84.3±5.6
104.7	79.6±5.1	51.4±3.4	45.5±3.3	66.3±4.7	81.8±5.3	90.0±5.5	101 ±6.5
114.5	99.2±6.3	104 ±6.4	116 ±8.2	115 ±7.3	116 ±7.2	109 ±6.7	104 ±6.7
124.2	120 ±7.7	176 ±11	211 ±13	180 ±11	163 ±10	142 ±8.5	125 ±8.0
133.7	139 ±9.0	247 ±15	301 ±19	272 ±17	204 ±15	176 ±11	149 ±9.5
143.1	158 ±10	323 ±20	394 ±24	338 ±21	264 ±16	217 ±13	191 ±12
152.4	165 ±11	369 ±22	477 ±29	427 ±28	324 ±23	262 ±16	236 ±15
157.0	163 ±11	402 ±24		455 ±29	351 ±25	275 ±17	

TABLE II. Differential cross sections $\sigma(\theta)$ of neutrons elastically scattered from carbon for E_n=4.25–4.91 MeV. The errors are rms absolute errors. The rms relative errors can be determined by unfolding the following systematic errors: E_n=3.03–5.15 MeV, $\Delta\sigma_{sys}$=5%; E_n=5.324–6.00 MeV, $\Delta\sigma_{sys}$=6%; E_n=6.25–6.94 MeV, $\Delta\sigma_{sys}$=7%. The uncertainty in scattering angle is estimated to be ±0.5°. Both θ and $\sigma(\theta)$ are in the center-of-mass system. All cross sections are in mb/sr.

θ° \ E_n / ΔE_n	4.25 MeV 70 keV	4.35 MeV 60 keV	4.45 MeV 65 keV	4.55 MeV 65 keV	4.64 MeV 65 keV	4.73 MeV 80 keV	4.91 MeV 37 keV
16.3	490 ±35	644 ±41	535 ±32	497 ±30	435 ±27	339 ±26	313 ±20
21.6	475 ±34	638 ±38	498 ±30	474 ±29	400 ±25	329 ±25	301 ±19
27.0	434 ±31		454 ±28		343 ±22		
32.4	390 ±28	479 ±29	425 ±25	336 ±21	327 ±20	275 ±19	239 ±16
37.8					259 ±16		
43.1	310 ±22	358 ±22	298 ±18	250 ±15	218 ±14	200 ±13	163 ±9.8
53.7	228 ±16	233 ±15	208 ±13	164 ±9.9	163 ±10	121 ±8.0	115 ±7.2
62.4	176 ±13	181 ±12	148 ±8.9	120 ±7.8	104 ±6.6	93.7±6.4	81.5±6.0
74.5	140 ±10	137 ±9.7	125 ±7.4	90.4±5.8	84.5±5.3	75.2±5.1	71.8±4.7
84.7	126 ±9.0	119 ±9.3	106 ±6.8	96.6±6.3	90.4±5.6	78.7±5.3	73.7±5.1
94.8	111 ±7.9	105 ±7.5	97.8±6.2	94.9±5.7	97.0±5.9	76.9±4.9	85.0±5.3
104.7	95.7±6.8	81.8±5.9	97.0±5.9	92.5±5.5	90.6±5.5	80.4±4.8	88.5±5.5
114.5	92.6±6.6	71.8±4.7	84.3±5.2	83.7±5.1	93.4±5.8	74.8±4.6	79.9±5.0
124.2	75.8±5.4	48.5±3.9	67.7±4.1	69.6±4.3	74.8±4.6	65.3±4.0	66.0±4.5
133.7	69.5±4.9	43.1±3.1	59.4±3.6	65.8±4.2	61.9±4.0	54.6±3.6	56.4±3.6
143.1	91.8±6.5	43.3±3.5	56.5±3.5	55.6±4.0	64.4±5.1	51.6±3.5	51.3±3.3
152.4	128 ±9.0		61.9±3.7	62.0±4.9	54.3±4.8	51.7±3.5	56.0±3.6
157.0		56.3±4.9		66.3±5.3			

TABLE III. Differential cross sections $\sigma(\theta)$ of neutrons elastically scattered from carbon for E_n=4.933–5.361 MeV. The errors are rms absolute errors. The rms relative errors can be determined by unfolding the following systematic errors: E_n=3.03–5.15 MeV, $\Delta\sigma_{sys}$=5%; E_n=5.324–6.00 MeV, $\Delta\sigma_{sys}$=6%; E_n=6.25–6.94 MeV, $\Delta\sigma_{sys}$=7%. The uncertainty in scattering angle is estimated to be ±0.5°. Both θ and $\sigma(\theta)$ are in the center-of-mass system. All cross sections are in mb/sr.

θ° \ E_n, ΔE_n	4.933 MeV [a] 35 keV	5.05 MeV 70 keV	5.15 MeV 70 keV	5.324 MeV [b] 37 keV	5.348 MeV [b] 37 keV	5.361 MeV [b] 37 keV
16.3		261 ±22	282 ±21	168 ±15		
21.6	321 ±23	266 ±20	246 ±17	170 ±14	208 ±17	351 ±31
32.4	219 ±19	199 ±15	219 ±15	143 ±11	179 ±15	311 ±26
43.1	155 ±14	153 ±10	144 ±9.1	103 ±7.5	138 ±11	216 ±17
53.7	109 ±9.7	106 ±7.4	101 ±6.4	81.0±6.0	106 ±7.6	153 ±11
64.2	87.9±9.1	77.1±5.4	69.9±4.6	75.8±5.5	90.1±6.7	104 ±8.1
74.5	73.5±7.9	63.8±4.5	63.3±4.2	67.1±5.0	83.5±6.1	86.5±6.6
84.7	76.7±7.8	70.7±4.5	68.3±4.5	62.2±4.5	79.7±5.7	78.3±6.0
94.8	88.0±8.7	76.9±5.5	77.8±4.9	62.9±4.5	75.6±5.4	75.8±5.6
104.7	93.4±9.7	82.7±4.9	82.0±5.1	57.5±4.1	62.4±4.7	69.4±5.0
114.5	87.5±9.0	79.6±5.1	76.4±4.9	53.7±4.0	52.5±3.8	63.2±4.6
124.2	80.9±8.6	68.9±4.4	67.4±4.3	38.7±3.1	38.2±2.6	51.8±3.9
133.7	67.4±7.3	59.4±4.0	59.2±3.9	31.7±2.8	30.4±2.4	41.4±3.4
143.1	59.4±6.4	48.7±3.3	49.5±3.3	28.9±2.6	37.2±2.8	39.2±3.2
150.8				40.1±3.1		
152.4	59.3±6.3	52.2±3.4	49.3±3.3		52.6±3.7	44.3±3.8
154.4				51.1±4.7		

[a] Energy measured relative to an assumed resonance energy of 4.933 MeV with an error of ±5 keV.
[b] Energy measured relative to an assumed resonance energy of 5.369 MeV with an error of ±5 keV.

TABLE IV. Differential cross sections $\sigma(\theta)$ of neutrons elastically scattered from carbon for E_n=5.377–6.250 MeV. The errors are rms absolute errors. The rms relative errors can be determined by unfolding the following systematic errors: E_n=3.03–5.15 MeV, $\Delta\sigma_{sys}$=5%; E_n=5.324–6.00 MeV, $\Delta\sigma_{sys}$=6%; E_n=6.25–6.94 MeV, $\Delta\sigma_{sys}$=7%. The uncertainty in scattering angle is estimated to be ±0.5°. Both θ and $\sigma(\theta)$ are in the center-of-mass system. All cross sections are in mb/sr.

θ° \ E_n, ΔE_n	5.377 MeV [a] 37 keV	5.47 MeV 40 keV	5.57 MeV 165 keV	5.78 MeV 155 keV	6.00 MeV 145 keV	6.250 MeV [b] 60 keV
16.3	378 ±30					
21.6	375 ±29	209 ±17	272 ±21	229 ±21	186 ±17	325 ±27
32.4	303 ±22	190 ±14	227 ±19	163 ±14	157 ±13	206 ±18
43.1	219 ±16	119 ±9.0	151 ±11	117 ±9.2	113 ±8.4	123 ±11
53.1	126 ±9.2	73.4±5.3	97.6±7.3	71.7±5.6	62.3±4.5	60.8±6.8
64.2	88.9±6.7	49.8±4.4	57.9±4.7	44.8±3.8	43.6±3.8	24.7±3.3
74.5	60.5±4.6	36.5±2.8	42.9±3.6	31.8±2.8	28.8±2.2	18.0±2.9
84.7	61.9±4.6	47.5±3.7	50.1±3.6	37.8±3.0	36.1±3.0	40.2±4.8
94.8	70.3±5.0	58.0±4.1	63.4±4.8	52.4±4.0	49.1±3.4	58.2±6.8
104.7	81.2±5.6	70.5±4.9	77.4±5.5	60.9±4.2	60.6±4.3	114 ±9.7
114.5	78.8±5.6	77.0±5.3	76.8±5.5	67.0±4.7	66.8±4.6	122 ±9.9
124.2	73.6±5.1	66.7±4.9	72.6±5.3	64.2±4.5	61.7±4.3	123 ±9.9
133.7	57.9±4.2	52.3±3.7	65.5±4.8	50.3±3.6	53.8±3.7	92.6±8.0
143.1	47.7±3.2	46.1±3.6	49.2±3.7	43.1±3.0	44.4±3.2	53.4±5.8
152.4	39.8±3.1	38.7±3.1	41.5±3.2	37.7±2.7	39.2±2.9	41.7±4.6

[a] Energy measured relative to an assumed resonance energy of 5.369 MeV with an error of ±5 keV.
[b] Energy measured relative to an assumed resonance energy of 6.293 MeV with an error of ±5 keV.

TABLE V. Differential cross sections $\sigma(\theta)$ of neutrons elastically scattered from carbon for $E_n = 6.291-6.94$ MeV. The errors are rms absolute errors. The rms relative errors can be determined by unfolding the following systematic errors: $E_n = 3.03-5.15$ MeV, $\Delta\sigma_{sys} = 5\%$; $E_n = 5.324-6.00$ MeV, $\Delta\sigma_{sys} = 6\%$; $E_n = 6.25-6.94$ MeV, $\Delta\sigma_{sys} = 7\%$. The uncertainty in scattering angle is estimated to be $\pm 0.5°$. Both θ and $\sigma(\theta)$ are in the center-of-mass system. All cross sections are in mb/sr.

$\theta°$ \ E_n, ΔE_n	6.291 MeV [a] 60 keV	6.333 MeV [a] 60 keV	6.523 MeV [a] 60 keV	6.563 MeV [a] 60 keV	6.606 MeV [a] 60 keV	6.94 MeV 130 keV
21.6	608 ±48	495 ±38	250 ±20	262 ±22	164 ±14	
32.4	296 ±23	308 ±25	174 ±14	180 ±15	89 ±10	90.8 ± 8.7
43.1	95.0 ± 8.0	107 ± 9.6	92.9 ± 7.8	86.2 ± 9.0	49.3 ± 4.4	68.1 ± 5.8
53.7	31.9 ± 3.6	33.2 ± 5.5	47.8 ± 4.6	40.9 ± 4.9	25.5 ± 3.1	44.7 ± 4.0
64.2	43.5 ± 3.9	44.5 ± 4.1	36.4 ± 4.3	27.3 ± 3.6	20.8 ± 2.3	34.8 ± 2.9
74.5	74.4 ± 6.1	71.9 ± 7.9	30.9 ± 3.3	26.9 ± 3.3		36.7 ± 3.1
84.7	111 ± 8.7	99.3 ± 7.6	33.3 ± 3.5	32.8 ± 3.8	39.7 ± 3.9	41.2 ± 3.2
94.8	145 ±11	87.6 ± 7.8	38.8 ± 3.8	43.8 ± 4.9	46.3 ± 4.8	49.6 ± 4.1
104.7	163 ±13	77.7 ± 6.0	36.7 ± 3.7	34.5 ± 3.8	39.6 ± 3.9	51.5 ± 4.1
114.5	188 ±15	67.7 ± 6.6	30.3 ± 3.0	24.0 ± 2.8		49.7 ± 4.2
124.2	157 ±12	75.2 ± 5.8	24.9 ± 2.9	22.1 ± 2.7	25.4 ± 2.7	41.1 ± 3.2
133.7	125 ± 9.6	76.6 ± 7.2	28.0 ± 2.9	21.0 ± 2.6	17.4 ± 2.0	28.9 ± 2.8
143.1	111 ± 8.7	84.9 ± 6.7	32.0 ± 3.1	23.0 ± 2.7	20.4 ± 2.3	23.8 ± 2.0
152.4	110 ± 8.7	95 ±13			15.8 ± 1.9	19.3 ± 1.8
154.2			40.0 ± 3.6	27.9 ± 3.1		

[a] Energy measured relative to an assumed resonance energy of 6.293 MeV with an error of ±5 keV.

formula used to calculate the fraction of detected neutrons that have been scattered only once, the above researchers made the approximation $\sigma_T(E) = \sigma_T(E_0)$, where σ_T is the total cross section, E_0 is the incident energy, and E is the neutron energy after scattering through an angle θ. In the present work the actual dependence of the total cross section on neutron energy, and hence on scattering angle, was introduced because of the large variation with energy in the vicinity of the resonances studied. Multiple-scattering corrections were generally less than 5%, the main exceptions being a few cross sections near 90° at 3.25, 3.46, and 3.67 MeV where the corrections were 20 to 75%. These cross sections were changing rapidly with angle and approaching zero near 90°.

The n-p total cross section values used for cross-section normalization were calculated with Gammel's semiempirical formula.[18] This formula reproduces precision n-p cross-section measurements in the energy range 0.1 to 20 MeV with an accuracy of better than 1%.

The differential cross sections for elastic scattering are given in Table I–V and are also shown in Figs. 3–7, along with the total cross section[4] in the corresponding energy region. The absolute errors (see Sec. II D) are plotted. The angular distributions for elastic scattering have been fitted by series of Legendre polynomials:

$$\sigma(E, \theta) = \sum_L B_L(E) P_L(\cos\theta),$$

using a least-squares criterion of goodness of fit. The expansion coefficients are tabulated in Table VI. Inelastic differential cross sections for the reaction $^{12}C(n, n)^{12}C^*_{4.43}$ were corrected for dead time and flux attenuation. The inelastic cross sections are given in Tables VII and VIII and are shown in Fig. 8. The solid curves are least-squares Lengendre-polynomial fits whose polynomial coefficients and uncertainties are listed in Table IX.

For each angular-distribution measurement the energy distribution of the neutrons incident upon the scatterer was calculated in a three-step process, taking into account the energy spread due to straggling in entrance foil and target gas, and the kinematic spread due to the finite size of the scatterer. The procedure is described in detail elsewhere.[23] The full width at half maximum (FWHM) of the energy distributions ranged from 35 to 165 keV, and the values are listed in Tables I–V and VII and VIII.

D. Errors

The following individual errors contributed to the rms errors in the cross sections. All errors are given as standard deviations (S.D.):

(1) Neutron monitor counts. S.D. ≤ 1%.

(2) Error in carbon scattering yield including statistics and uncertainty in background subtraction. 2% ≤ S.D. ≤ 12%.

(3) Error in the angular-distribution shape due to

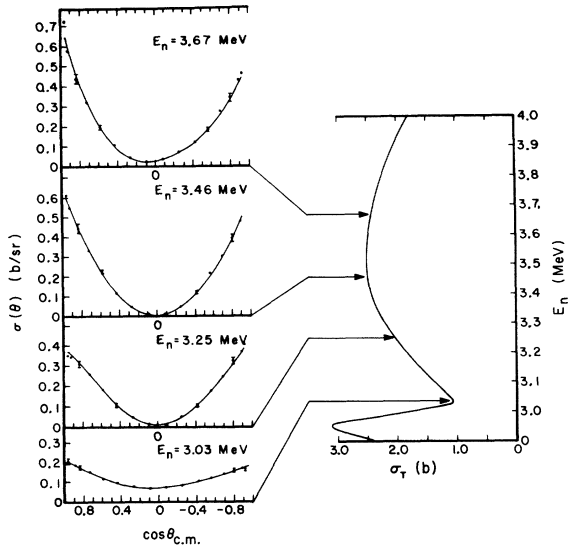

FIG. 3. Angular distributions of neutrons elastically scattered from carbon in the region of the 3.5-MeV resonance. The total cross section curve from BNL 325 (Ref. 4) is also given in Figs. 3–7 to show the energies of the angular distributions relative to the resonances in σ_T. The error bars shown are the absolute rms errors. The smooth lines through the data points are the fits from the phase-shift analysis.

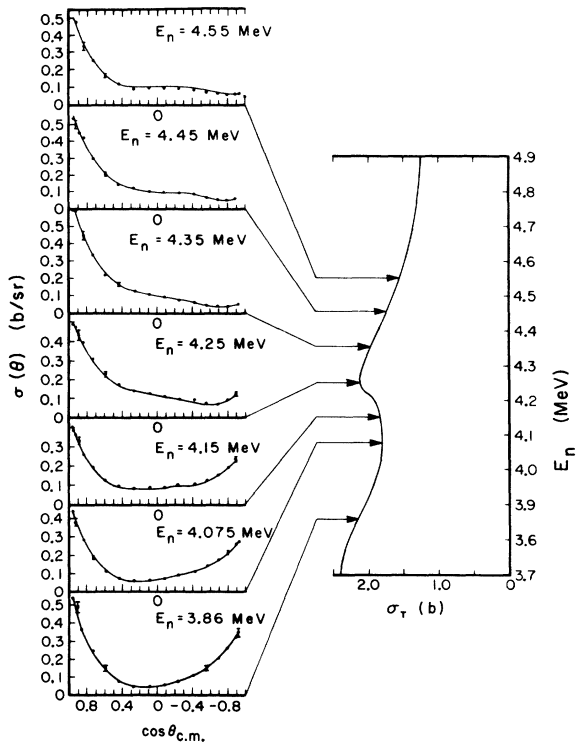

FIG. 4. Angular distributions of neutrons elastically scattered from carbon in the region of the 4.26-MeV resonance. (See caption of Fig. 3 for other information.)

the uncertainty in the energy dependence of the detector efficiency. S.D. $\cong$ 2%.

(4) Multiple-scattering correction, S.D. < 1%, except for a few points near 90° where S.D. $\leq$ 15% (see Sec. IIC and below).

(5) Error in n-p scattering yield, including statistics and uncertainty in background subtraction. S.D. $\cong$ 3.5%.

(6) Error in the normalization of the cross-section magnitudes due to the uncertainty in the energy dependence of the efficiency. S.D. $\cong$ 3 to 6%.

(7) Flux-attenuation correction. 0.4 $\leq$ S.D. $\leq$ 1.1%.

(8) n-p total cross section. S.D. $\leq$ 1%.

The angular-resolution correction and the weights of the carbon and polyethylene scattering samples were assumed to be known exactly, since each had an S.D. < 0.2%. Items (1)–(4) in the above list combine to give the relative error in each data point in a given angular distribution, while items (5)–(8) determine the probably range of any systematic error in the absolute magnitude of the cross sections. All eight error contributions combined give the absolute rms errors in the cross sections.

For bombarding energies up to and including 4.15 MeV the absolute error (S.D.) in the individual data points of the elastic cross sections is smaller than 6.5%, except for data points around 90° for bombarding energies of 3.25, 3.46, 3.67, and 3.86 MeV where there were large multiple-scattering corrections and the absolute error ranged up to 17%. From 4.25 to 5.15 MeV, the absolute error

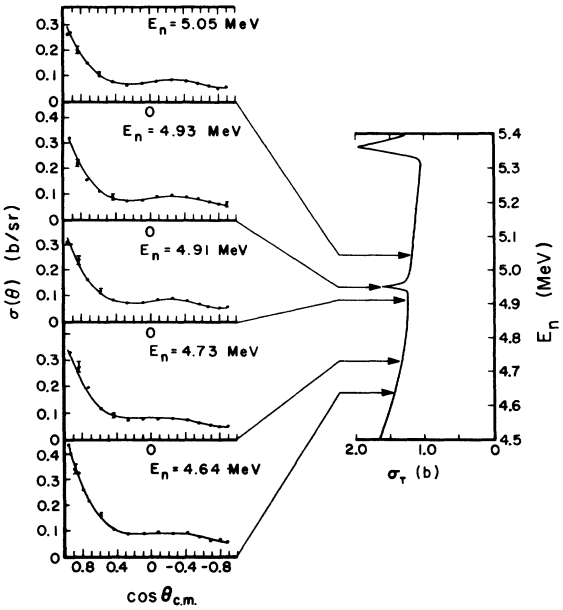

FIG. 5. Angular distributions of neutrons elastically scattered from carbon in the region of the 4.95-MeV resonance. (See caption of Fig. 3 for other information.)

on most of the data points is still less than 6.5%, but in many of the angular distributions there are a few data points with errors ranging from 7 to 9%. The angular distribution at 4.933 MeV has errors of about 10% except at forward angles, because of poor counting statistics. Between 5.32 and 6.00 MeV, the absolute error ranges from 7 to 9%. At 6.25-MeV bombarding energy and above the absolute errors mostly range from 7 to 11%, with an occasional error as large as 15%. The gradual change in accuracy is due to decreasing cross sections and increasing background.

The angle-integrated cross sections (see Fig. 16) are, on the average, systematically higher than published total cross sections by amounts increasing from 3 to 7% with increasing energy. The normalizations of the cross sections at 21 of the bombarding energies scattered throughout the whole energy range were checked by remeasurement. The reproducibility of these checks, as well as the agreement of the angle-integrated cross sections with the published total cross sections, indicates that the magnitude of the cross sections reported here is correct to within ± 5% up to 5.2 MeV and ±7% at the higher energies. The scattering-angle error is ±0.5°.

Items (1)–(3) and (5)–(8) were used to calculate the S.D.'s of the inelastic cross sections. The uncertainty in the elastic cross section due to errors in the detector efficiency curve at energies corresponding to inelastically scattered neutrons ranged from 6 to 11% for the angular distributions at 6.250, 6.291, 6.330, 6.523, 6.563, and 6.606 MeV, and 20 to 50% at 5.78, 6.00, and 6.94 MeV. Multiple-scattering and angular-resolution corrections were not attempted, and the corresponding errors were neglected.

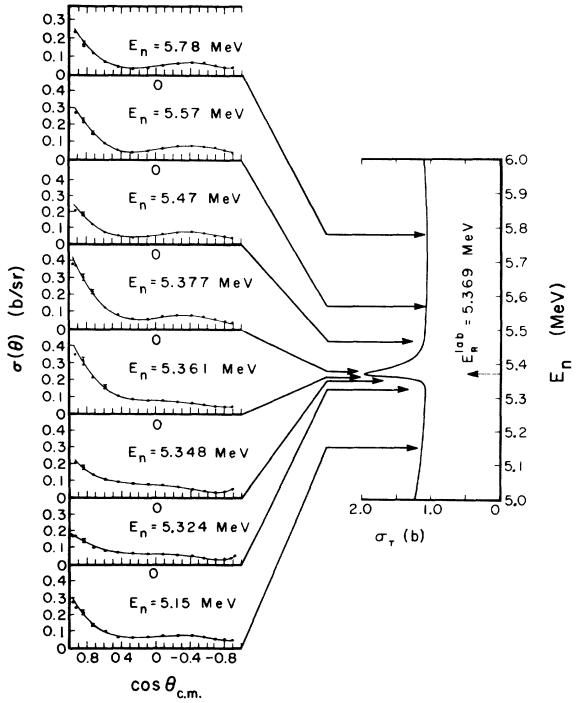

FIG. 6. Angular distributions of neutrons elastically scattered from carbon in the region of the 5.35-MeV resonance. (See caption of Fig. 3 for other information.)

III. PHASE SHIFTS

A. Analysis

The center-of-mass differential cross section for the scattering of neutrons from spin-zero nuclei can be written as[24]

$$\sigma(\theta)=\lambda^2(|f_c|^2+|f_i|^2), \tag{1}$$

where

$$f_c=\sum_{l=0}^{\infty}P_l(\cos\theta)[(l+1)e^{i\delta_l^+}\sin\delta_l^+ + l e^{i\delta_l^-}\sin_l^-], \tag{2}$$

$$f_i=\sin\theta\sum_{l=0}^{\infty}P_l'(\cos\theta)(e^{i\delta_l^+}\sin\delta_l^+ - e^{i\delta_l^-}\sin\delta_l^-), \tag{3}$$

and $\delta_l^{\pm}=\delta(l, J=l\pm\frac{1}{2})$ is the phase shift of the par-

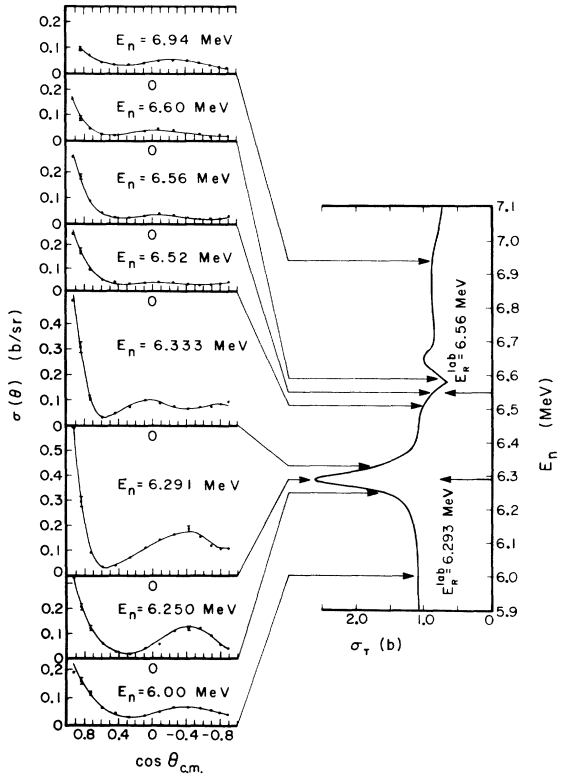

FIG. 7. Angular distributions of neutrons elastically scattered from carbon in the region of the 6.29- and 6.56-MeV resonances. (See caption of Fig. 3 for other information.)

tial wave of total angular momentum $J=l\pm\frac{1}{2}$. Other quantities in Eqs. (2) and (3) are:

$P_l(\cos\theta)$ = Legendre polynomial of order l,

$P_l'(\cos\theta)=dP_l(\cos\theta)/d(\cos\theta)$,

$\lambda\!\!\!^{-}=\hbar/\mu v$,

where μ is the reduced mass of the system and v is the relative velocity.

When only the elastic scattering channel is open, the phase shift can be expressed as the sum of two real quantities[25]

$$\delta_l^{\pm}=\delta_l^J=\phi_l^J+\beta_l^J, \tag{4}$$

where ϕ_l^J is the contribution from potential scattering [sometimes assumed to be hard-sphere scattering; i.e., $\phi_l=-\tan^{-1}(F_l/G_l)$ where F_l and G_l are regular and irregular solutions of the radial wave equation] and β_l^J is due to scattering from compound-nucleus resonances. In an energy region where there is only one resonance of a given l and J it is usual to make the single-level approximation[25] for β_l^J:

$$\beta_l^J=\tan^{-1}\left[\frac{\Gamma_l^J}{2(E_R-E)}\right], \tag{5}$$

where Γ_l^J is the total resonance width, E_R is the resonance energy, and E is the neutron bombarding energy. The energy dependence of the level shift and the width were neglected, since all levels to which Eq. (5) was applied were relatively narrow.

If nonelastic channels are open, the phase shifts become complex quantities; i.e.,

$$\delta_l^J=\Delta_l^J+i\gamma_l^J .$$

Approximate expressions for the real part of the phase shift Δ_l^J and the damping parameter $A_l^J=e^{-2\gamma_l^J}$

TABLE VI. Legendre-polynomial coefficients from least-squares fits to elastic scattering data in Tables I–V. The expansion is given by $\sigma(\theta)=\sum B_L P_L(\cos\theta)$. The B_L's are in mb/sr; energies are in MeV. The uncertainties in the coefficients were determined from the relative errors in the cross sections.

E_n	B_0	B_1	B_2	B_3	B_4	B_5	B_6	B_7
3.03	114.5±1.2	3.37±2.4	87.3±3.0	14.1±3.5	−8.1±4.3			
3.25	164.4±1.7	−20.3 ±4.1	280.1±4.9	−11.2±4.1	−42.7±5.0			
3.46	207.6±2.7	4.3 ±6.7	406.7±8.7	27.8±10.6	−6.0±7.4	22.4±7.6		
3.67	203.1±2.4	29.6 ±5.7	388.8±7.4	57.6±6.1	41.1±7.1			
3.86	175.4±2.1	32.6 ±5.0	295.1±6.6	74.2±5.6	55.5±6.5			
4.075	147.2±1.4	10.1 ±3.1	206.2±4.0	59.5±3.8	58.7±4.4			
4.15	148.2±1.7	23.4 ±3.8	172.2±5.3	40.8±5.3	64.5±6.1			
4.25	169.8±2.5	149.7 ±5.1	147.4±6.5	36.3±8.0	57.1±8.2	−26.4±9.2		
4.35	170.3±2.0	229.6 ±4.1	173.4±5.4	101.9±5.6	68.3±5.2			
4.45	154.9±1.4	177.0 ±3.0	138.9±3.7	92.6±3.9	53.5±4.0			
4.55	136.6±1.4	143.6 ±2.9	128.3±3.8	102.5±3.9	58.6±3.9			
4.64	126.8±1.2	123.4 ±2.5	105.2±3.4	97.5±3.6	46.1±4.2			
4.73	108.1±1.4	102.4 ±3.1	89.5±4.1	78.7±4.0	39.9±3.9			
4.91	103.1±1.1	81.7 ±2.3	74.8±2.9	69.9±3.6	40.0±3.7	−14.6±4.1		
4.93	106.7±2.4	79.2 ±4.4	74.5±6.2	83.5±7.1	41.3±8.1			
5.05	94.8±1.3	68.5 ±2.8	60.8±3.6	61.4±4.3	25.5±4.2	−16.1±4.4		
5.15	92.9±1.1	68.6 ±2.4	62.6±3.1	68.1±3.7	30.1±3.7	−10.3±4.1		
5.324	71.3±0.9	48.6 ±1.9	34.8±2.7	16.6±3.0	33.4±3.6	−10.0±3.4	13.0±3.9	
5.348	86.1±1.3	68.8 ±2.9	45.0±3.7	16.3±4.4	38.6±4.1	−11.1±4.1		
5.361	112.7±2.0	127.4 ±4.9	100.8±6.3	67.5±7.3	37.2±6.2	−9.0±5.7		
5.377	109.6±1.4	115.0 ±3.1	106.4±3.9	100.5±4.6	25.0±4.3	−13.6±4.3		
5.47	75.4±1.0	52.2 ±2.5	58.5±3.1	73.3±3.8	17.9±3.4	−16.1±3.5		
5.57	88.7±1.3	73.0 ±3.1	78.1±4.0	88.7±4.7	17.7±4.2	−12.1±4.4		
5.78	70.3±1.3	52.1 ±3.4	62.1±4.3	70.5±5.0	14.2±4.4	−12.9±4.1		
6.00	66.3±1.1	42.8 ±3.0	55.9±3.8	65.5±4.4	10.8±3.8	−13.1±3.7		
6.25	93.0±1.7	49.6 ±3.5	92.1±5.6	157.6±5.8	38.2±7.5	−8.9±6.5	32.5±7.5	
6.29	156.0±1.9	74.2 ±5.4	163.4±6.9	264.6±9.7	208.9±8.1	85.2±9.9	81.6±7.4	15.6±8.5
6.33	116.3±2.1	91.1 ±6.0	156.6±8.1	154.7±11.3	168.4±10.3	77.7±11.5	14.7±8.0	−20.1±8.5
6.52	58.3±0.9	64.5 ±2.0	83.1±2.6	67.2±3.2	55.9±3.1	13.5±3.2		
6.56	55.3±1.2	71.6 ±2.7	84.6±3.5	79.8±4.2	65.3±4.1	19.3±4.1		
6.61	42.1±0.9	38.2 ±2.0	34.0±2.5	55.0±2.9	48.3±3.1	14.5±3.7		
6.94	48.3±1.0	29.1 ±2.6	17.2±3.3	39.3±3.9	16.7±3.3	−6.6±3.3		

TABLE VII. Differential cross sections of neutrons inelastically scattered from ^{12}C for E_n=5.78–6.333 MeV. The errors are rms absolute errors. Because of the larger contribution to the errors from the uncertainty in the detector efficiency, the relative error cannot be separated from the absolute error. The uncertainty in scattering angle is estimated to be ±0.5°. Both θ and $\sigma(\theta)$ are in the center-of-mass system. All cross sections are in mb/sr.

E_n	5.78 MeV		6.00 MeV		6.250 MeV [a]		6.291 MeV [a]		6.333 MeV [a]	
ΔE_n	155 keV		145 keV		60 keV		60 keV		60 keV	
	θ°	$\sigma(\theta)$	θ°	$\sigma(\theta)$	θ°	$\sigma(\theta)$	θ°	$\sigma(\theta)$	θ°	$\sigma(\theta)$
	24.1	28 ± 9	23.7	26 ± 7	23.4	47.5 ± 6.2	23.4	41.8 ± 4.9	23.4	24.3 ± 2.8
	35.9	25 ± 8	35.4	32 ± 8	35.0	41.1 ± 6.1	34.9	35.1 ± 4.0	34.9	24.6 ± 4.1
	47.6	26 ± 8	46.9	25 ± 6	46.4	37.6 ± 4.8	46.4	23.5 ± 3.1	46.3	36.1 ± 4.7
	59.0	29 ± 9	58.3	24 ± 6	57.7	28.1 ± 3.9	57.6	29.7 ± 3.0	57.5	27.4 ± 3.9
	70.2	22 ± 6	69.4	29 ± 8	68.7	22.4 ± 5.2	68.6	29.3 ± 2.6	68.5	30.8 ± 2.7
	81.1	28 ± 9	80.2	22 ± 7	79.5	19.6 ± 3.1	79.3	24.1 ± 2.7	79.2	30.4 ± 4.2
	91.6	28 ± 9	90.6	35 ± 11	89.9	16.7 ± 3.7	89.8	19.8 ± 2.1	89.6	25.1 ± 2.4
	101.8	30 ± 14	100.8	33 ± 14	100.1	10.5 ± 4.0	100.0	24.3 ± 3.7	99.8	28.7 ± 4.6
	111.6	26 ± 14	110.7	35 ± 14	109.9	14.8 ± 4.2	109.8	23.4 ± 3.4	109.7	26.7 ± 3.3
	121.1	27 ± 14	120.2	42 ± 18	119.5	20.1 ± 5.3	119.3	25.7 ± 3.7	119.3	33.6 ± 5.7
	130.2	43 ± 23	129.3	37 ± 18	128.7	23.2 ± 5.5	128.6	28.7 ± 4.2	128.5	31.3 ± 3.9
	139.0	26 ± 14	138.2	45 ± 22	137.6	15.4 ± 6.0	137.6	33.7 ± 5.0	137.6	32.2 ± 5.7
	147.6	65 ± 36	146.9	42 ± 22	146.4	19.4 ± 4.0	146.4	33.4 ± 4.8	146.3	35.4 ± 4.8
	155.9	59 ± 32	155.4	50 ± 27	155.0	25.4 ± 5.5	155.0	37.3 ± 5.0	155.0	41.1 ± 6.6

[a] Energy measured relative to an assumed resonance energy of 6.293 MeV with an error of ±5 keV.

as given by Duval, Barnard, and Swint[26] are

$$\Delta_l^J = \phi_l^J + \tfrac{1}{2}\tan^{-1}\left[\frac{a_l^J \sin 2\beta_l^J}{1 - a_l^J + a_l^J \cos 2\beta_l^J}\right], \quad (6)$$

$$A_l^J = \alpha_l^J[(1 - a_l^J + a_l^J \cos 2\beta_l^J)^2 + (a_l^J \sin 2\beta_l^J)^2]^{1/2}, \quad (7)$$

where α_l^J and ϕ_l^J represent A_l^J and Δ_l^J in an energy region without resonances, and the quantities in the square brackets are now the resonant forms related to the unbound energy levels of the compound nucleus.[27] Also,

$$a_l^J \equiv \Gamma_{el}/\Gamma,$$

where Γ_{el} is the width for elastic scattering, and Γ is the total width of a single level. In the vicinity of a single resonance the energy dependence of β_l^J is still given by Eq. (5). A discussion of the

TABLE VIII. Differential cross sections of neutrons inelastically scattered from ^{12}C for E_n=6.523–6.94 MeV. The errors are rms absolute errors. Because of the larger contribution to the errors from the uncertainty in the detector efficiency, the relative error cannot be separated from the absolute error. The uncertainty in scattering angle is estimated to be ±0.5°. Both θ and $\sigma(\theta)$ are in the center-of-mass system. All cross sections are in mb/sr.

E_n	6.523 MeV [a]		6.563 MeV [a]		6.606 MeV [a]		6.94 MeV	
ΔE_n	60 keV		60 keV		60 keV		130 keV	
	θ°	$\sigma(\theta)$	θ°	$\sigma(\theta)$	θ°	$\sigma(\theta)$	θ°	$\sigma(\theta)$
	23.2	32.4 ± 3.6	23.2	45.6 ± 4.3	23.2	24 ± 3		
	34.7	33.0 ± 3.6	34.6	45.7 ± 4.4	34.6	27 ± 5	34.3	12 ± 2
	46.1	36.3 ± 4.2	46.0	46.5 ± 4.2	46.0	24 ± 2	45.6	15 ± 2
	57.2	27.6 ± 2.8	57.2	38.1 ± 4.1	57.1	20 ± 3	56.6	12 ± 2
	68.2	28.9 ± 3.4	68.1	34.0 ± 3.5	68.0	22 ± 3	67.5	12 ± 2
	78.9	21.4 ± 2.5	78.8	32.3 ± 3.9	78.7	18 ± 4	78.2	7.2 ± 1.4
	89.3	16.9 ± 2.1	89.2	20.8 ± 2.5	89.1	13 ± 2	88.6	8.1 ± 1.6
	99.4	18.4 ± 2.8	99.4	23.5 ± 3.1	99.3	14 ± 3	98.7	15 ± 3
	109.3	21.5 ± 3.2	109.2	24.0 ± 3.7	109.1	19 ± 4	108.6	11 ± 3
	118.9	26.3 ± 3.5	118.8	27.5 ± 4.2			118.2	17 ± 4
	128.2	29.6 ± 4.4	128.1	32.8 ± 4.6	128.0	18 ± 4	127.5	18 ± 4
	137.2	30.6 ± 4.1	137.1	37.7 ± 5.3	137.1	25 ± 3	136.6	24 ± 6
	146.1	30.8 ± 4.3	146.0	34.1 ± 5.0	146.0	22 ± 6	145.6	26 ± 7
	156.6	25.1 ± 3.4	156.3	29.0 ± 4.3	154.7	13 ± 5	154.3	20 ± 5

[a] Energy measured relative to an assumed resonance energy of 6.293 MeV with an error of ±5 keV.

shapes of the resonant forms of Eqs. (6) and (7) is given by Morris, Kerr, and Ophel.[28]

The theoretical cross sections $\sigma_{th}(\theta_i)$ calculated from Eq. (1) were compared with the experimental cross sections $\sigma_{exp}(\theta_i)$, and a best fit to each angular distribution was determined by a minimum χ^2 given by

$$\chi^2 = \sum_{i=1}^{N} \left[\frac{\sigma_{th}(\theta_i) - \sigma_{exp}(\theta_i)}{\mathrm{err}(\theta_i)} \right]^2 , \qquad (8)$$

where N is the number of data points in the angular distribution and $\mathrm{err}(\theta_i)$ is the S.D. in $\sigma_{exp}(\theta_i)$.

A computer program was written to search on the phase shifts, one at a time in one-degree steps, in a process of continuous iteration, until no further reduction in χ^2 resulted. In analyzing the angular distributions below 3.5 MeV, the phase shifts of Wills *et al.*[7] were inserted as starting parameters in the search program. For the analysis of angular distributions at successively higher energies, extrapolated phase shifts from preceding distributions were inserted as starting parameters. In this way the requirements of proper physical behavior for the phase shifts were maintained. Partial waves with $l=3$ were used only above 4.64 MeV, although the error in the Δ_3^+ was determined at all energies. In the vicinity of the 6.29-MeV resonance, $l=4$ partial waves were also included in the program, but were found to be unnecessary.

For angular distributions measured in the vicinity of one of the narrow resonances at 4.933, 5.369, 6.293, or 6.56 MeV with a neutron energy distribution which was a significant fraction of the width Γ of the resonance, it was necessary to average the variation of the theoretical differential cross section over the neutron energy distribution in order to calculate χ^2. This procedure has been used by Fowler.[29] The neutron energy distribution (see Sec. IIC) was approximated in this averaging process to within 10% by a Gaussian which was truncated to a total width of 2 times the FWHM.

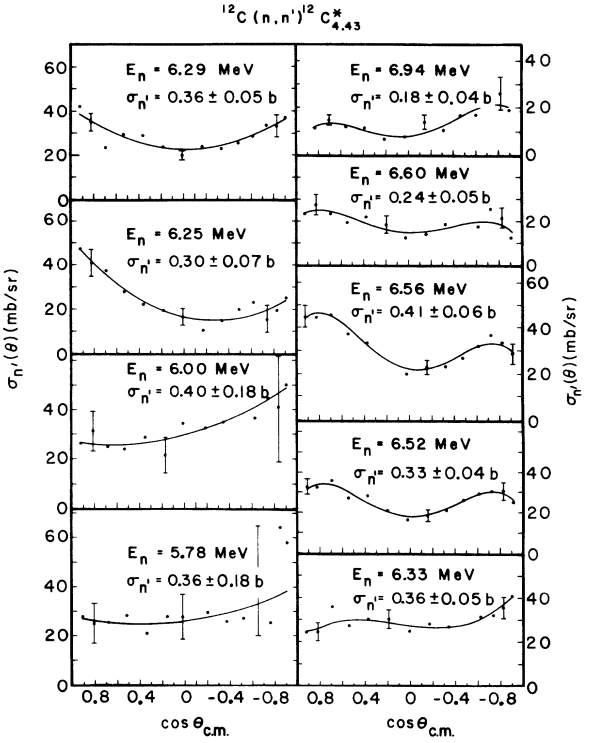

FIG. 8. Angular distributions of neutrons inelastically scattered from the 4.43-MeV state of ^{12}C. The error bars show the absolute rms errors, and the solid lines are the least-squares fits to the data by series of Legendre polynomials.

For these same angular distributions, the parameters a_l^J, ϕ_l^J, α_l^J, and the mean neutron energy E_n were searched on whenever knowledge of them was thought to be uncertain. The values of a_l^J and ϕ_l^J determined by the search are given in Table X. These values of a_l^J agree well with the values calculated from the integrated cross sections for elas-

TABLE IX. Legendre-polynomial coefficients and angle-integrated cross sections from least-squares fits to inelastic scattering cross sections given in Tables VII and VIII. The cross sections are expanded in the form $\sigma(\theta) = \sum B_L P_L(\cos\theta)$. The B_L's are in mb/sr; energies are in MeV; $\sigma_{n'}$ is in b. The uncertainties in the coefficients are calculated from the absolute rms errors of the cross sections. The errors on the integrated cross sections include the uncertainty in the detection efficiency.

E_n	B_0	B_1	B_2	B_3	B_4	$\sigma_{n'}$
5.78	28.7±3.4	−6.1±6.4	5.6±7.4			0.36±0.14
6.00	32.4±3.6	−11.7±6.6	8.3±7.2			0.41±0.15
6.250	23.7±1.2	12.5±2.3	15.6±2.9			0.30±0.07
6.291	28.2±0.9	0.5±1.8	11.7±2.3			0.35±0.05
6.333	29.6±1.0	−4.6±1.9	4.3±2.5	−7.3±3.1		0.37±0.05
6.523	25.9±0.9	2.9±1.6	8.3±2.0	0.1±2.6	−10.6±3.0	0.33±0.05
6.563	32.5±1.0	8.8±2.0	11.3±2.5	−0.2±3.4	−11.3±3.7	0.41±0.05
6.606	18.9±0.9	3.1±1.6	3.8±2.3	1.8±3.0	−7.8±3.2	0.24±0.05
6.94	13.4±0.9	−5.6±1.9	5.2±2.8	−0.4±2.7	−7.6±3.4	0.17±0.04

TABLE X. Real phase shifts and damping parameters derived from elastic scattering cross sections. The damping parameters $A_l^{\pm}$ are only tabulated when not equal to 1.000, which is the case for all $E_n > 5.15$ MeV. For the four highest energy resonances, the resonant phase shift and damping parameter were calculated from the quantities ϕ_l^J, a_l^J, Γ, E_n, and E_R. Resonant phase shifts are given in degrees as $\Delta_1^{\pm} + 180°$ (mod 180°). Potential phase shifts are in degrees and are unmodified.

E_n (MeV)	Δ_0 A_0	Δ_1^+ A_1^+	Δ_1^- A_1^-	Δ_2^+ A_2^+	Δ_2^- A_2^-	Δ_3^+ A_3^+	Δ_3^- A_3^-	ϕ^J	a_l^J	Γ_{lab} (keV)	χ^2
3.03	105 ± 7	4 ± 5	4 ± 4	178 ± 2	30 ± 6	0 ± 2	0				4.2
3.25	75 ± 7	173 ± 5	171 ± 6	173 ± 3	50 ± 6	0 ± 2	0				6.1
3.46	79 ± 6	166 ± 8	175 ± 5	2 ± 3	77 ± 10	0 ± 2	0				10.5
3.67	81 ± 6	167 ± 6	177 ± 6	170 ± 3	100 ± 7	0 ± 2	0				5.5
3.86	74 ± 5	168 ± 2	174 ± 4	171 ± 2	114 ± 4	0 ± 2	0				2.4
4.075	69 ± 9	168 ± 2	2 ± 7	171 ± 2	122 ± 5	0 ± 2	0				2.0
4.15	55 ± 8	169 ± 2	17 ± 4	170 ± 2	115 ± 7	0 ± 2	0				6.5
4.25	54 ± 9	169 ± 2	56 ± 4	170 ± 2	120 ± 8	0 ± 2	0				12.0
4.35	66 ± 6	167 ± 2	112 ± 4	170 ± 2	130 ± 4	0 ± 2	0				4.9
4.45	51 ± 8	167 ± 2	122 ± 4	172 ± 2	126 ± 4	0 ± 2	0				4.8
4.55	50 ± 8	166 ± 2	130 ± 3	171 ± 2	129 ± 7	0 ± 2	0				7.7
4.64	35 ± 10	164 ± 2	131 ± 3	172 ± 2	126 ± 7	0 ± 2	0				10.2
4.73	31 ± 10	167 ± 2	136 ± 3	174 ± 1	129 ± 9	0 ± 2	0				11.9
4.91	28 ± 9	168 ± 3	142 ± 3	172 ± 2	126 ± 7	1 ± 3	0				4.1
4.933[a]	44 ± 9	77	150 ± 5	172 ± 2	137 ± 3	0 ± 3	0 ± 2	−13 ± 5	1.0	5	2.6
4.933[b]	39 ± 8	164 ± 3	49	173 ± 2	132 ± 3	0 ± 3	1 ± 2	−41 ± 5	1.0	5	3.0
5.05	36 ± 10	168 ± 2	144 ± 3	173 ± 2	132 ± 8	1 ± 3	0 ± 2				6.0
5.15	32 ± 8	166 ± 2	143 ± 3	174 ± 2	132 ± 8	0 ± 2	0 ± 2				9.5
5.324[c]	31 ± 8	0 ± 6	148 ± 4	175 ± 2	134 ± 3	2 ± 2	3 ± 3	−12 ± 5	0.70 ± 0.10	28	7.3
	0.93 ± 0.10	0.97 ± 0.06		0.90 ± 0.10	0.93 ± 0.16						
5.348[c]	44 ± 8	12 ± 6	151 ± 4	173 ± 2	137 ± 3	0 ± 2	3 ± 2	−12 ± 7	0.70 ± 0.10	28	2.8
	0.90 ± 0.07	0.87 ± 0.10		0.93 ± 0.07							
5.361[c]	36 ± 10	39 ± 19	131 ± 6	177 ± 2	134 ± 4	0 ± 2	9 ± 2	−9 ± 10	0.70 ± 0.10	28	3.5
	0.71 ± 0.16	0.61 ± 0.18		0.81 ± 0.16							
5.377[c]	42 ± 8	130 ± 21	137 ± 7	173 ± 2	139 ± 4	0 ± 2	6 ± 3	−8 ± 10	0.70 ± 0.10	28	6.1
	0.71 ± 0.16	0.61 ± 0.18		1.00 ± 0.07							
5.47	30 ± 8	162 ± 5	143 ± 4	175 ± 2	135 ± 4	2 ± 3	0 ± 2				6.3
	1.00 ± 0.07	1.00 ± 0.06	0.93 ± 0.10	0.93 ± 0.03	0.87 ± 0.03						
5.57	30 ± 10	160 ± 4	141 ± 4	174 ± 2	131 ± 8	1 ± 2	0 ± 2				2.8
	0.93 ± 0.13		1.00 ± 0.10	1.00 ± 0.07							
5.78	18 ± 10	163 ± 7	151 ± 6	175 ± 2	131 ± 8	2 ± 2	0 ± 2				2.3
	0.93 ± 0.16		1.00 ± 0.1	1.00 ± 0.07							
6.00	20 ± 10	162 ± 7	151 ± 6	176 ± 2	132 ± 3	2 ± 2	0 ± 2				4.9
	0.97 ± 0.16		1.00 ± 0.1	0.97 ± 0.16							
6.250[d]	33 ± 10	155 ± 5	150 ± 8	173 ± 6	142 ± 6	27 ± 6	0 ± 4	1 ± 5	0.70 ± 0.10	58	10.9
	0.76 ± 0.26			0.93 ± 0.24	0.97 ± 0.15	0.84 ± 0.06	0.93 ± 0.06				
6.291[d]	37 ± 8	154 ± 4	141 ± 7	162 ± 3	138 ± 5	94 ±	19 ± 5	4 ± 12	0.70 ± 0.10	58	4.2
	1.00 ± 0.06			1.00 ± 0.1	1.00 ± 0.1	0.51 ± 0.20					
6.333[d]	35 ± 10	155 ± 4	138 ± 7	164 ± 3	133 ± 6	165 ± 6	7 ± 4	10 ± 5	0.70 ± 0.10	58	6.3
	1.00 ± 0.06			0.97 ± 0.21	0.97 ± 0.15	0.84 ± 0.06					
6.523[e]	33 ± 9	162 ± 4	142 ± 5	175 ± 3	145 ± 4	176 ± 2	175 ± 3	−159 ± 7	0.40 ± 0.10	40	5.4
	0.87 ± 0.06			0.76 ± 0.25	1.00 ± 0.1	1.00 ± 0.1					
6.563[e]	174 ± 19	165 ± 4	152 ± 5	167 ± 3	139 ± 3	176 ± 2	0 ± 3	−167 ± 7	0.40 ± 0.10	40	4.8
	0.31 ± 0.17			1.00 ± 0.2	1.00 ± 0.1	1.00 ± 0.1					
6.606[e]	13 ± 10	169 ± 4	150 ± 5	169 ± 2	144 ± 3	176 ± 2	6 ± 3	−158 ± 10	0.40 ± 0.10	40	5.9
	0.93 ± 0.06	0.87 ± 0.30	0.97 ± 0.30	0.10 ± 0.2	0.84 ± 0.30	0.90 ± 0.12					
6.94	24 ± 8	168 ± 4	148 ± 6	173 ± 2	140 ± 4	0 ± 2	3 ± 5				2.3
			0.97 ± 0.20	1.00 ± 0.1	1.00 ± 0.1						

[a] $E_R = 4.933$ MeV; $l = 1$, $J = \frac{3}{2}$.
[b] $E_R = 4.933$ MeV; $l = 1$, $J = \frac{1}{2}$.
[c] $E_R = 5.369$ MeV; $l = 1$, $J = \frac{3}{2}$.
[d] $E_R = 6.293$ MeV; $l = 3$, $J = \frac{7}{2}$.
[e] $E_R = 6.558$ MeV; $l = 0$, $J = \frac{1}{2}$.

tic and inelastic scattering at the energies where both were measured. This provides an independent check of the search method of obtaining a_l^J.

The variation of E_n was kept within its experimental error of 5 keV with respect to E_R. The values of E_R and Γ_{lab} which were used for these four narrow resonances are given in Sec. II B. These values were not searched on, except for $E_R = 6.56$ MeV. All possible combinations of l and J for resonant phase shifts were tried for every resonance, within the limitations on l given above. Except for the angular distributions at 4.933 MeV and near 5.35 MeV, only one combination at each resonance gave acceptable fits to all angular distributions in the vicinity of the resonance.

The energy-averaging procedure was used in calculating fits at mean laboratory energies of 4.933, 5.324, 5.348, 5.361, 5.377, 6.250, 6.291, 6.333, 6.523, 6.563, and 6.606 MeV. Resonant phase shifts and damping parameters for the above energies were calculated from a^J, ϕ_l^J, E_n, E_R, and Γ_{lab}.

B. Errors in Phase Shifts

S.D.'s in the phase shifts (both real and imaginary parts above the inelastic threshold) and in a_l^J were determined by the method of Anderson *et al.*,[30] except that a more conservative criterion for determining the errors was used here; i.e., phase-shift changes which caused χ^2 to increase to $\chi^2 + 2$ rather than $\chi^2 + 1$ were taken as the S.D. in the phase shift. For the nonresonant phase shifts obtained by energy averaging of the calculated cross sections, the errors were calculated by an approximation procedure that gave essentially the same result as the Anderson method, but at a great saving in computer time. Typical errors in the phase shifts are plotted in Fig. 9. Errors in the potential phases were also calculated in the same manner. For the resonant phase shifts in the energy-averaged regions, the S.D. of the real part of the phase shift and the associated damping parameter were calculated from the S.D.'s of ϕ_l^J, a_l^J, and E_n.

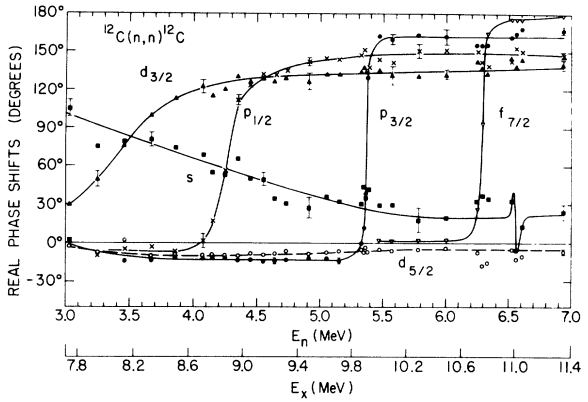

FIG. 9. Phase shifts obtained from least-squares fits to neutron elastic scattering data in the incident neutron energy range 3 to 7 MeV. The phase-shift change of 180° for the 4.93-MeV resonance has been omitted because it is uncertain whether it should appear in Δ_1^+ or Δ_1^- and also because the resonance is so narrow that it does not affect the results at nearby energies. Δ_0 and Δ_2^- are actually plotted as $\Delta_0 + \pi$ and $\Delta_2^- - \pi$ in order to show all the phase shifts on the same 180° scale. The lines are only smooth free-hand curves showing the trends of the phase shifts. The bottom scale gives the excitation energies in the compound nucleus ^{13}C.

C. Results of Phase-Shift Analysis

Values of the real part of the phase shifts and damping parameters at 32 energies are given in Table X. Where damping parameters are not listed the values are 1 because either the inelastic channel is closed, or within the errors of the experiment the smaller values were not required. The fits calculated from the phase-shift analysis are shown as solid lines in Figs. 3–7.

The variation with energy of the real parts of the phase shifts is shown in Fig. 9. Free-hand smooth curves have been drawn to indicate, within the experimental errors, approximately how the phase shifts change with energy. Phase shifts for the data at 4.933 MeV were omitted from the figure because two independent sets, using either a $\frac{1}{2}^-$ or $\frac{3}{2}^-$ resonant phase shift, gave satisfactory fits to the data.

The $p_{1/2}$ phase shift between 3.25 and 4.91 MeV was fitted with an expression of the form

$$\delta_1^{1/2} = \phi_1^{1/2} + \tan^{-1}\frac{\Gamma}{2(E_R - E)}$$

in order to determine E_R and Γ for the resonance in this region. A straight-line approximation for $\phi_1^{1/2}$ was used,

$$\phi_1^{1/2} = -K_1 E + K_2 .$$

The parameters K_1, K_2, Γ, and E_R were adjusted to give an optimum fit to the data by minimizing a χ^2 function similar to that in Eq. (8). The best values arrived at for the above parameters are:

$$E_R = 4.26 \pm 0.02 \text{ MeV},$$

$$\Gamma = 200 \pm 40 \text{ keV},$$

$$K_1 = 13°/\text{MeV},$$

$$K_2 = 30°.$$

The best fit to the $p_{1/2}$ phase shift is shown in Fig. 10.

This is the only resonance for which such a dispersion fit was possible. The 3.5-MeV $d_{3/2}$ reso-

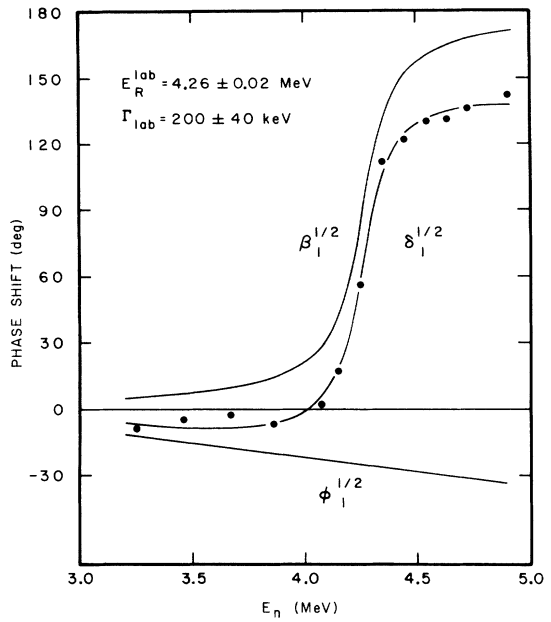

FIG. 10. Least-squares fit of the single-level approximation to the experimental $\delta_1^{1/2}$ phase shift at the 4.26-MeV resonance, where $\delta_1^{1/2}=\phi_1^{1/2}+\beta_1^{1/2}$. The parameters of the resonant phase shift $\beta_1^{1/2}$ and the background phase shift $\phi_1^{1/2}$ are given in the figure.

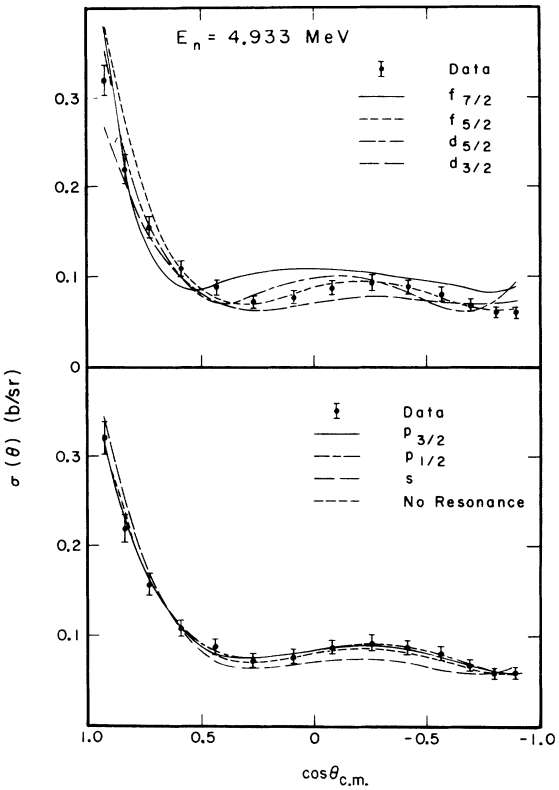

FIG. 11. Least-squares fits to the 4.933-MeV angular distribution. The assumed resonant phase shift labels each of the curves. A total width of 5 keV and pure elastic scattering were assumed. The fits for a $p_{1/2}$ resonance and for no resonance are shown only where they differ significantly from the $p_{3/2}$ curve. From the fits, the resonance is thought to be either $p_{1/2}$ or $p_{3/2}$.

nance interferes with the 2.95-MeV $d_{3/2}$ resonance, for which no data were taken. All the other resonances were measured with a neutron-energy resolution that was an appreciable fraction of the resonance width, and in the energy-averaging procedure of the phase-shift analysis *a priori* assumptions of a single-level Breit-Wigner shape, and width and resonant energy from the work of Cierjacks *et al.*[5] were made.

The measured angular distribution at 4.933 MeV was fitted under the assumption that $\Gamma_{lab}=5$ keV and $a_i^J=1$ for the resonance at 4.933 MeV. Using the energy-averaging procedure as described above with a neutron energy distribution of 35-keV width, all l, J combinations through $l=3$ were attempted for the resonant phase. For each l, J combination the nonresonant phase shifts were searched upon with a restriction that they should not deviate significantly beyond their expected S.D.'s from those values given by the solid lines in Fig. 9 at 4.93 MeV. Figure 11 shows the resulting fits to the data. Fits assuming a $p_{1/2}$ or no resonance are

TABLE XI. Sets of phase shifts giving best fits to the 4.933-MeV resonance for various assumed resonant phases. The phase shifts are given in degrees, as $\Delta_i^{\pm}+180°$ (mod 180°).

Resonant phase \ Phase shift	s	$p_{1/2}$	$p_{3/2}$	$d_{3/2}$	$d_{5/2}$	$f_{5/2}$	$f_{7/2}$	χ^2
s	128	146	167	131	170	0	0	41
$p_{1/2}$	39	49	164	132	173	1	0	3.0
$p_{3/2}$	44	150	77	137	172	0	0	2.6
$d_{3/2}$	38	140	168	44	171	0	0	36
$d_{5/2}$	33	138	169	138	82	0	0	66
$f_{5/2}$	35	145	168	136	173	90	0	27
$f_{7/2}$	34	140	169	138	173	0	92	120
No resonance	43	142	166	132	172	0	0	6.1

shown only where they deviate significantly from the curve for a $p_{3/2}$ resonance. Values of the phase shifts and χ^2 are listed in Table XI for each curve.

Almost equally good fits to the four angular distributions in the neighborhood of the 5.35-MeV resonance were obtained by assuming that it was either a $p_{1/2}$ or $p_{3/2}$ resonance, with the $p_{3/2}$ fits having a slightly smaller χ^2. Because of the spin limitations, $J \geq \frac{3}{2}$, from the work of Fossan *et al.*,[1] we assign a spin and parity of $\frac{3}{2}^-$ to the 9.90-MeV excited state of ^{13}C. A phase-shift analysis of unpublished $^{12}C(n, n)^{12}C$ measurements by Hermsen[31] gives the same assignment. Only the results of the fit with a $p_{3/2}$ resonance are shown in Fig. 9 and Table X.

For the resonance at 6.56 MeV, the width Γ_{lab} is 40 keV.[5] Since the neutron energy spreads were 60 keV for the three angular distributions nearest this resonance, the theoretical cross sections had to be energy averaged over large fractions of the phase-shift anomaly. Hence, a large part of the assumed phase-shift curve entered explicitly into each attempted fit. Good fits could be obtained for the s-wave phase-shift curve shown in Fig. 9, but not for a "normal" s-wave resonant phase shift which increased through 180° with increasing energy, nor for a resonance in any other partial wave. This unusual behavior for a resonant phase shift has been observed elsewhere[26,28] and is expected[26] whenever the elastic partial width is less than half of the total width, i.e., $a_l^J < \frac{1}{2}$.

Several resonance energies between 6.52 and 6.63 MeV were tried because it was not known how to accurately assign a resonance energy to the dip in the total cross section (see Fig. 7). The energy arrived at, 6.558 MeV, yielded an over-all best fit to the three angular distributions, while maintaining reasonable values for the nonresonant phase shifts. It was thought to be reasonable to ignore the effect of the state of 11.09-MeV excitation energy ($E_R = 6.65$ MeV) on the angular distributions in this region, since its width is 5 keV.[32]

In Fig. 9 it can be seen that for resonant energies above 5 MeV there is some tendency at several resonances for the nonresonant phase shifts to deviate from their off-resonance values. This phenomenon has also been observed under similar circumstances in the phase-shift analysis of $^{16}O(p,p)^{16}O$ by Salisbury and Richards.[33] It can probably be attributed to one or more of the following causes:

(1) The accuracy of the data decreases with in-

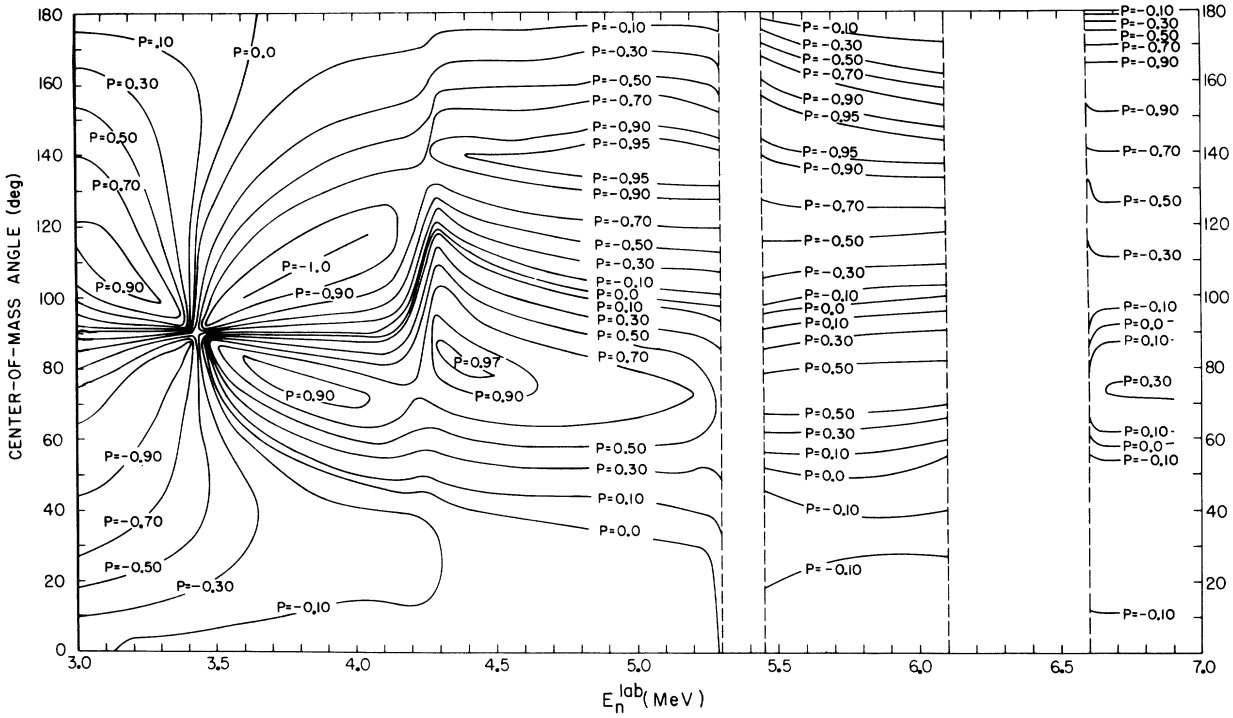

FIG. 12. Contour diagram of the predicted polarization of neutrons elastically scattered from carbon as a function of scattering angle and incident neutron energy from 3 to 7 MeV. The contours are labeled by the polarization magnitude and were calculated from phase-shift values read from the smooth lines in Fig. 9. The blank regions near 5.35 and 6.4 MeV are very complicated and are shown on expanded scales in Figs. 13 and 14.

creasing bombarding energy.
(2) The inelastic channel is treated in an approximate manner in the analysis.
(3) The influence of possible broad levels at energies above the region of investigation with the same J^{π} as the observed resonances was neglected.
(4) The length of time required by the energy averaging of the theory plus the increased number of parameters prevented refining the fits as much as at lower energies.
(5) The energy-averaging procedure itself involved approximations including that for the shape of the neutron energy distribution.
(6) In the assumptions about the energy dependence of the resonant phases, the exact resonance energies are uncertain, especially for the $s_{1/2}$ resonance at 6.56 MeV.

In spite of the small anomalies in the nonresonant phase shifts, the assigned resonant spins and parities are the only ones compatible with the data.

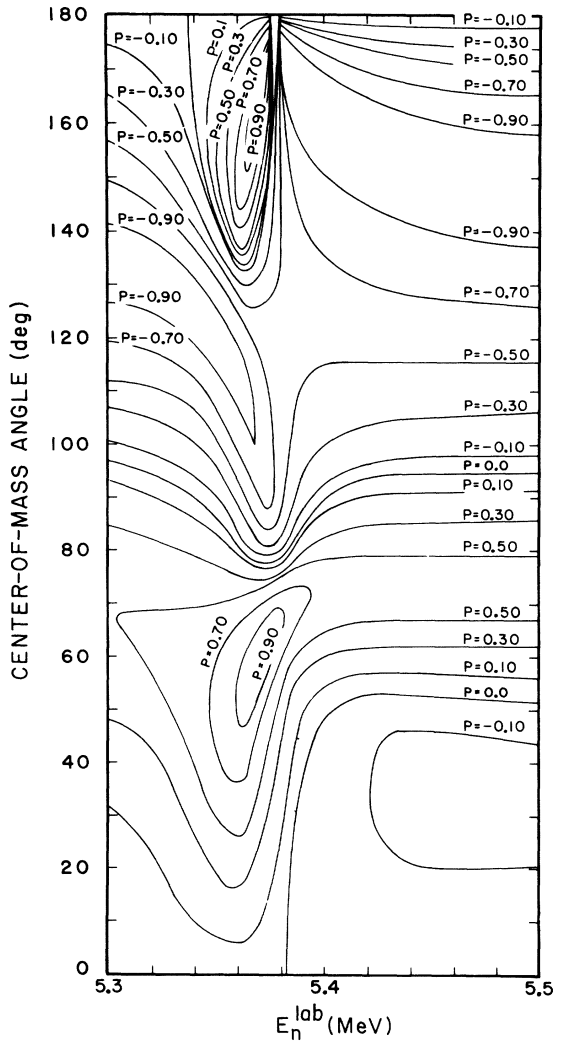

FIG. 13. Contour diagram of the predicted polarization of neutrons elastically scattered from carbon as a function of scattering angle in the region of the 5.35-MeV resonance.

IV. CALCULATED POLARIZATIONS

The polarization of neutrons elastically scattered from spinless nuclei is conveniently expressed in terms of the scattering amplitudes, Eqs. (2) and (3), as[34]

$$P(\theta)=\frac{2\,\mathrm{Im}[f_i(\theta)f_c^*(\theta)]}{|f_i(\theta)|^2+|f_c(\theta)|^2}\,.$$

A computer program calculated constant-polarization contours, i.e., $P(\theta,E)=K$ where $-1\leq K\leq+1$, from phase-shift values read from the smooth lines in Fig. 9 and smooth lines through the experimental values of the damping parameters. The results are shown in Figs. 12, 13, and 14. Note that the calculated polarization is larger than 0.9 over wide energy regions for fixed angles, which suggests that carbon may be useful as a polarization analyzer in these regions.

Comparisons of these calculated polarizations with the measurements of Gorlov, Lebedeva, and Morozov,[35] Bucher *et al.*,[36] Kelsey, Kobayashi, and Mahajan,[37] Wenzel and Steuer,[38] and Miller and Biggerstaff[39] are shown in Fig. 15 as solid lines. The phase shifts used in calculating the solid lines were varied within their S.D.'s so as to minimize the difference between a calculated polarization and ±1. The polarizations given by the dashed lines were determined in this manner. These lines delimit the regions within which measured polarizations would be compatible with the present results, and also indicate the great sensitivity of the calculated polarization to small changes in the phase shifts, especially above 6 MeV.

From a coupled-channel calculation, Reynolds *et al.*[40] have obtained polarizations to compare with the data of Kelsey, Kobayashi, and Mahajan[37] at 4.38 MeV; Gorlov, Lebedeva, and Morozov[35]; and Wenzel and Steuer.[38] Their calculated polarizations differ from the polarizations calculated from the phase-shift curves in Fig. 9 by less than 0.2 in all three cases, and less than 0.1 for the 4.38-MeV data of Kelsey, Kobayashi, and Mahajan.[37]

V. DISCUSSION

A. Comparison with Previous Data

The measured cross sections presented here can be compared with the results of earlier experiments[6-13] at a few common or almost common

bombarding energies. When compared with the results of MST[6] and Wills *et al.*[7] at $E_n = 3.03$, 3.25, and 3.67 MeV, there is agreement within the combined experimental errors at most angles. Where this is not true, differences in the experimental conditions such as the detector geometry and small shifts in bombarding energy make the disagreement plausible.

At 4.1 MeV the present results agree within the experimental errors with Walt and Beyster[10] at forward angles, and are slightly higher than Wills *et al.*[7] at most angles. The discrepancy with these earlier experiments is most noticeable in the angular region $90° \leq \theta_{lab} \leq 120°$, where the present results are larger than the previous ones. This angular distribution was measured on four separate occasions over a five month period and each time the same result was obtained at these angles. The coupled-channels calculation of Reynolds *et al.*,[40] which was made without knowledge of our measurements, fits our data better at these angles than it does that of the earlier experiments. At 5 MeV the angular distribution of Hill[11] agrees well with the present data except for $\theta > 110°$ where our results are uniformly 30 mb/sr larger.

Perey and Kinney[9] have measured angular distributions at neutron energies of 5.04, 5.56, 6.01, and 7.03 MeV which can be compared with the work presented here. The results of the two sets of measurements are somewhat different at most energies and angles, but most of the differences are smaller than the combined experimental errors. Only at 5.56 MeV, where the Perey and Kinney cross sections are 40% lower than the present results at 32.4° and are 20% higher near 105°, are the differences outside the experimental errors. Since all the above differences follow no systematic pattern, it appears that they truly represent the state-of-the-art accuracy for time-of-flight measurements.

The largest disagreement between previous experiments and the present data is at 5.6 MeV, where the cross-section values of Braley and Cook[12] are 30% lower at forward angles and up to 300% larger in the backward direction than our cross sections at 5.57 MeV. Because of their 400-keV energy spread, there is less justification for comparing the 7.0-MeV angular distribution of Beyster, Walt, and Salmi[13] with the present results. In spite of this difference in experimental conditions, there is agreement within the experimental errors at most angles. No comparison with other measurements was attempted, since the neutron energy spread was too large or else unknown.

In general, it can be said that the angular distributions reported here are in good qualitative agreement, i.e., same general shape, with almost

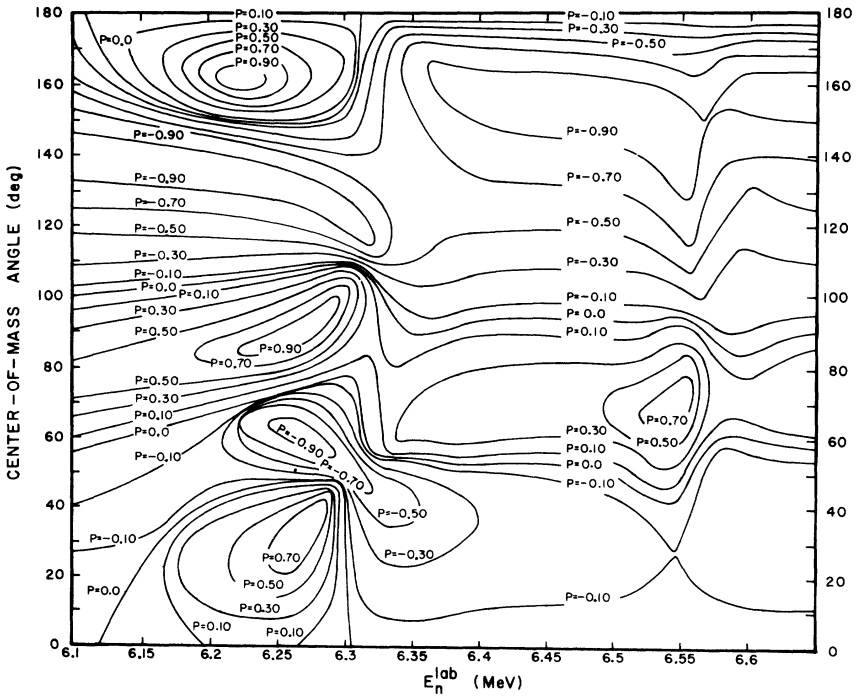

FIG. 14. Contour diagram of the predicted polarization of neutrons elastically scattered from carbon as a function of scattering angle in the region of the 6.29-MeV resonances.

all the previous work in the same energy region. The quantitative agreement varies but is also, in general, fairly good, especially when one considers the cruder apparatus and many approximations that were used in many of the earlier experiments, which span a period of 15 yr. These quantitative differences are reflected in some of the differences in the derived phase shifts, which are discussed below.

Values of the total cross section can be obtained by summing the angle-integrated partial cross sections given in Tables VI and IX. In the region near the 5.35-MeV resonance where the inelastic cross section was not measured, the elastic cross section was multiplied by $\Gamma/\Gamma_{el} = 1.43$, obtained in the phase-shift analysis (see Table X), to obtain the total cross section. These total-cross-section values are shown in Fig. 16, together with the recommended total-cross-section curve[4] from *Neutron Cross Sections* (BNL 325), and a curve representing the data, except near the narrow resonances, of Schwartz, Heaton, and Schrack[41] at the National Bureau of Standards. The present results agree better with the work of Schwartz, Heaton, and Schrack[41] than with the BNL 325 curve from 3 to 4.9 MeV, although they are systematically higher than both curves from 4.35 to 4.64 MeV. The recent work of Stoler

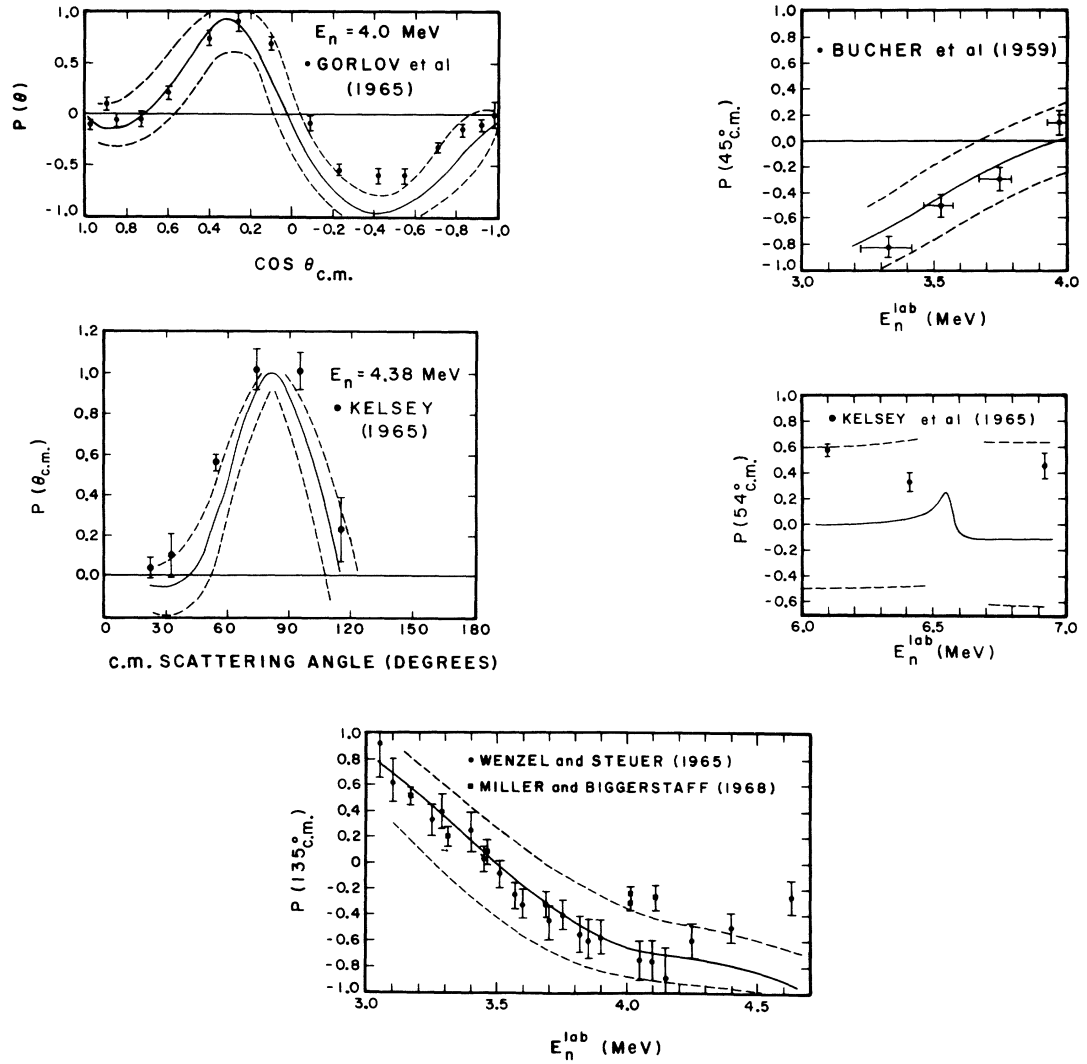

FIG. 15. A comparison of the presently available $^{12}C + n$ polarization data to the polarization predicted by the results of the present experiment (solid line). The data are from the measurements of Gorlov, Lebedeva, and Morozov (Ref. 35), Bucher *et al.* (Ref. 36), Kelsey, Kobayashi, and Mahajan (Ref. 37), Wenzel and Steuer (Ref. 38), and Miller and Biggerstaff (Ref. 39). The regions between the dashed lines give the ranges of polarization values that are obtained when the phase shifts are varied within their standard deviations.

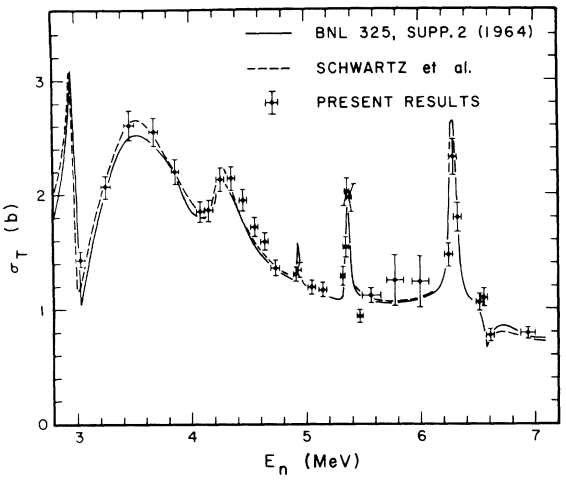

FIG. 16. A comparison of the angle-integrated cross sections from the present experiment with the measured total cross sections given in Refs. 4 and 41. The error bars represent the absolute rms errors. The four points on the 5.35-MeV resonance were obtained by multiplying the angle-integrated elastic cross sections by $(a_1^{3/2})^{-1}$.

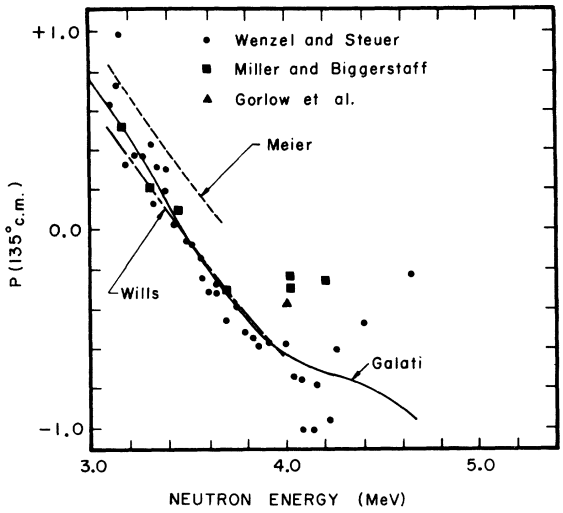

FIG. 18. A comparison of the polarizations predicted from the phase shifts of MST (Ref. 6), Wills *et al.* (Ref. 7), and the present experiment with the data of Wenzel and Steuer (Ref. 38).

et al.[42] also agrees very well with the National Bureau of Standards curve. From 4.7 to 5.6 MeV there is very good agreement between the present work and the BNL 325 curve, except at 5.47 MeV where no inelastic contribution is included, and at 4.95 MeV where our energy spread was greater than the width of the resonance. Above 5.6 MeV, the present results fluctuate about the BNL 325 recommended curve, but generally differ by less than 15%. The uncertainty in the magnitude of the inelastic cross section at 5.78 and 6.00 MeV is very large because of uncertainty in the neutron detection efficiency at very low neutron energy, and is the reason for the large error bars at those

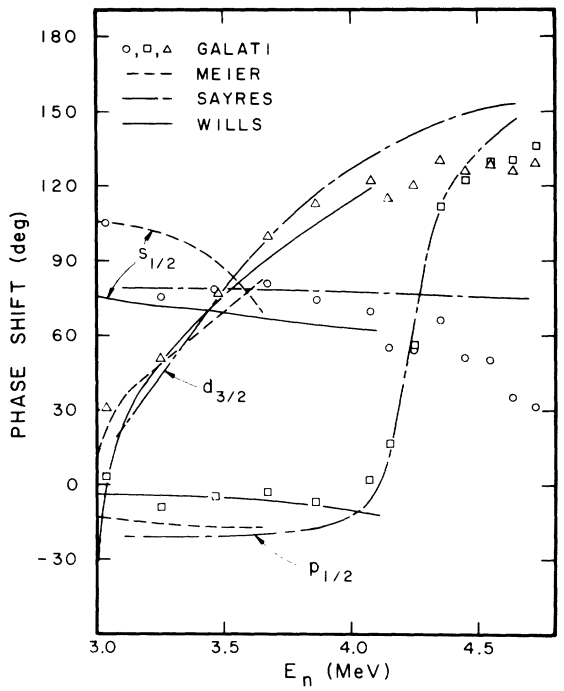

FIG. 17. A comparison of the $s_{1/2}$, $p_{1/2}$, and $d_{3/2}$ phase shifts determined in the present experiment with those from the work of MST (Ref. 6), Wills *et al.* (Ref. 7), and Lister and Sayres (Ref. 8).

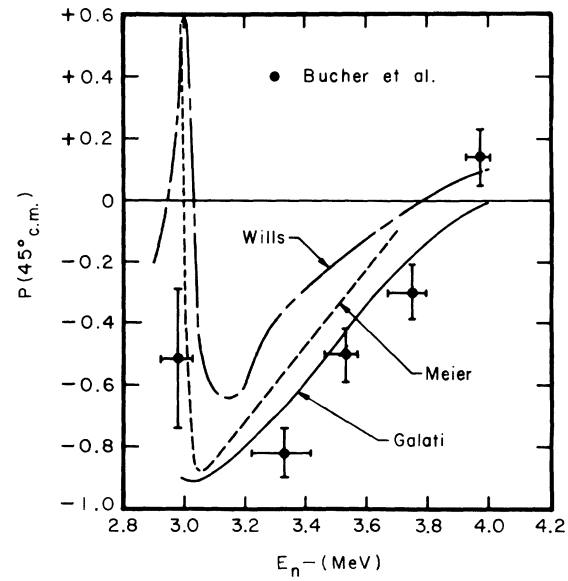

FIG. 19. A comparison of the polarizations predicted from the phase shifts of MST (Ref. 6), Wills *et al.* (Ref. 7), and the present experiment with the data of Bucher *et al.* (Ref. 36).

TABLE XII. Level parameters of states in ^{13}C.

E_R [a] (MeV)	E_x (^{13}C) [b] (MeV)	J^π	Γ_{lab} (keV)	Γ_{el}/Γ	ϕ_l^J (deg)
3.67[c]	8.33	$\frac{3}{2}^+$	1690 [c]	1.00	c
4.26 ± 0.02	8.88	$\frac{1}{2}^-$	200 ± 40	1.00	−25 ± 3
4.933 ± 0.003 [d]	9.501	$(\frac{1}{2}^-, \frac{3}{2}^-)$	± 5.5 [d]	1.00	(−41, −13)
5.369 ± 0.003 [d]	9.903	$\frac{3}{2}^-$	28 ± 3 [d]	0.70 ± 0.10	−10 ± 3
6.293 ± 0.003 [d]	10.756	$\frac{7}{2}^-$	57 ± 4 [d]	0.70 ± 0.10	+5 ± 5
6.558 ± 0.008	11.001	$(\frac{1}{2}^+)$	40 ± 4 [d]	0.40 ± 0.10	−161 ± 5

[a] E_R is the laboratory neutron energy at resonance, i.e., where $\beta_l^J = 90°$.
[b] $E_x = (\frac{12}{13})E_R + 4.947$ MeV.
[c] Quantities obtained from Ref. 7 as best values available. ϕ_l^J was not determined in this work.
[d] Quantities obtained from Ref. 5.

two energies. In general, the integrated cross-section values agree with the previously measured total cross section to within the errors of the experiments.

B. Phase Shifts and Polarization

For more than 10 years there has been a running discussion[43-45] over the differences in the phase shifts derived by MST[6] and by Wills *et al.*[7] The two sets of phase shifts have been tested by comparing measured polarizations and differential cross sections with the same quantities calculated from the phase shifts. Some measurements[46,47] agree better with the Meier phase shifts and others[44,45,48] agree better with those of Wills. Recently, a third set of phase shifts in the same energy region has been published by Lister and Sayres.[8]

In Fig. 17 is shown a comparison of the s, $p_{1/2}$, and $d_{3/2}$ phase shifts derived in this and previous experiments in the energy region where there is an overlap. All three phase shifts show significant differences from one experiment to another, with the largest disagreements in the d wave above 4 MeV and in the s wave. The other phase shifts were found to be small in all four experiments, and the differences are not significant.

The most sensitive way to test the correctness of phase shifts derived from angular distributions is to compare the predicted polarization with the measured polarization. This comparison is made in Figs. 18 and 19 between all the presently available data and the polarizations calculated from the phase shifts of Wills *et al.*, MST, and the present experiment.

At 135°, the present results fit slightly better than those of Wills *et al.* and much better than those of MST. Between 4.0 and 4.2 MeV there is a large disagreement in the three available sets of data and the predicted polarization lies in between the extremes of the data. Above 4.3 MeV the polarization at 135° predicted by the present phase shifts disagrees badly with the data. It is peculiar that the measured polarization changes magnitude so rapidly near 4.6 MeV, since there is no resonance in this energy region. At 45°, the phase shifts of this experiment fit the polarization measurements of Bucher *et al.*[36] much better than those of either Wills or Meier.

C. Resonance Parameters

The resonance parameters for the ^{13}C compound nucleus derived from the data of this experiment are given in Table XII. The spin and parity of the broad $E_x = 8.3$ MeV level were previously determined by MST[6], Wills *et al.*,[7] and by Lister and Sayres.[8] An analysis to determine the resonant energy and width of this level from the present results has not been carried out, since it requires data on the low-energy tail of this resonance and on the narrower resonance at 2.95 MeV which were not obtained in the present work. The results of Wills *et al.*,[7] which do not include a value for $\phi_2{}^{3/2}$ are given for this level as the best values presently available.

The $\frac{1}{2}^-$ assignment for the 8.9-MeV level was also made by Lister and Sayres.[8] They reported a width Γ_{lab} of 195 ± 54 keV and a resonance energy of 4.25 ± 0.02 MeV, both of which agree with the values in Table XII within the experimental errors.

The $(\frac{1}{2}^-, \frac{3}{2}^-)$ assignment of this work to the state at $E_x = 9.50$ MeV agrees with the tentative $\frac{3}{2}^-$ assignment of Fleming *et al.*[49] from a $^{15}N(p, {}^3He)^{13}C$ experiment, and also with the limitation $J > \frac{1}{2}$ of Fossan *et al.*[1] The $\frac{3}{2}^-$ and $\frac{7}{2}^-$ assignments to the 9.90- and 10.75-MeV excited states are consistent with the spin limitations for these states of Fossan *et al.*[1] This is the first time that a definite J^π assignment has been given to either of these levels. Since the present assignments were first announced,[50] Wittwer, Clerc, and Beer[51] have confirmed the $\frac{3}{2}^-$ assignment to the 9.90-MeV state by electron scattering measurements. A tentative $(\frac{1}{2}^+)$ assignment was given to the 11.00-MeV level by James, Jones, and Wilkinson[52] in agreement with the present work.

ACKNOWLEDGMENTS

The authors wish to thank Dr. G. C. Dutt and Dr. A. W. Obst for their valuable assistance in taking the data, and the University of Kentucky Computing Center for supplying computer time for data reduction and analysis.

---

*Work supported in part by the National Science Foundation. Preliminary accounts of this work appeared in Bull. Am. Phys. Soc. 11, 831 (1966); 13, 1388 (1968); in, Proceedings of the Third International Symposium on Polarization in Nuclear Reactions, Madison, Wisconsin, 1970 (unpublished).

†Present address: Raff Associates, Inc., Silver Springs, Maryland.

‡Work performed in partial fulfillment of the requirements for Ph.D. degree.

[1]D. B. Fossan, R. L. Walter, W. E. Wilson, and H. H. Barschall, Phys. Rev. 123, 209 (1961).

[2]K. Tsukada and T. Fuse, J. Phys. Soc. Japan 15, 1994 (1960).

[3]R. L. Becker and H. H. Barschall, Phys. Rev. 102, 1384 (1956).

[4]*Neutron Cross Sections*, compiled by J. R. Stehn, M. D. Goldberg, B. A. Magurno, and R. Wiener-Chasman, Brookhaven National Laboratory Report No. BNL 325 (U. S. GPO, Washington D. C., 1964), 2nd ed., Suppl. No. 2.

[5]S. Cierjacks, Kernforschungszentrum Karlsruhe, Institut für Angewandte Kernphysik, private communication.

[6]R. W. Meier, P. Scherrer, and G. Trumpy, Helv. Phys. Acta 27, 577 (1954).

[7]J. E. Wills, Jr., J. K. Bair, H. D. Cohn, and H. B. Willard, Phys. Rev. 109, 891 (1958).

[8]D. Lister and A. Sayres, Phys. Rev. 143, 745 (1966).

[9]F. G. Perey and W. E. Kinney, Oak Ridge National Laboratory Report No. ORNL-4441, 1969 (unpublished).

[10]M. Walt and J. R. Beyster, Phys. Rev. 98, 677 (1955).

[11]R. W. Hill, Phys. Rev. 109, 2105 (1957).

[12]J. E. Braley and C. W. Cook, Phys. Rev. 118, 808 (1960).

[13]J. R. Beyster, M. Walt, and E. W. Salmi, Phys. Rev. 104, 1319 (1956).

[14]*Angular Distributions in Neutron Induced Reactions*, compiled by D. I. Garber, L. G. Strömberg, M. D. Goldberg, D. E. Cullen, and V. M. May, Brookhaven National Laboratory Report No. BNL-400 (U. S. GPO, Washington, D. C., 1970), 3rd ed., Vol. I, $Z = 1$ to 20.

[15]L. Cranberg, T. A. Oliphant, J. Levin, and C. D. Zafiratos, Phys. Rev. 159, 969 (1967); L. Cranberg, R. A. Fernald, F. S. Hahn, and E. F. Shrader, Nucl. Instr. Methods 12, 335 (1961).

[16]R. Batchelor, W. B. Gilboy, A. D. Purnell, and J. H. Towle, Nucl. Instr. Methods 8, 146 (1960).

[17]ATJ graphite (reactor grade) 99.999% natural carbon; loaned by Oak Ridge National Laboratory.

[18]J. L. Gammel, in *Fast Neutron Physics Part II*, edited by J. B. Marion and J. L. Fowler (Interscience, New York, 1963), p. 2209.

[19]L. Cranberg and J. S. Levin, Los Alamos Scientific Laboratory Report No. LA-2177, January 1959 (unpublished).

[20]J. Blok and C. C. Jonker, Physica 18, 809 (1952).

[21]M. Walt and H. H. Barschall, Phys. Rev. 93, 1062 (1954).

[22]J. D. Reber and J. D. Brandenberger, Phys. Rev. 163, 1077 (1967); J. D. Reber, Ph.D. dissertation, University of Kentucky, 1967 (unpublished).

[23]W. Galati, Ph.D. dissertation, University of Kentucky, 1969 (unpublished).

[24]C. L. Critchfeld and D. C. Dodder, Phys. Rev. 76, 602 (1949).

[25]A. M. Lane and R. G. Thomas, Rev. Mod. Phys. 30, 257 (1958).

[26]J. S. Duval, Jr., A. C. L. Barnard, and J. B. Swint, Nucl. Phys. A93, 164 (1967).

[27]There are two typographical errors in Eq. (8), Ref. 26 where the equation labeled as Eq. (7) in this paper is given.

[28]J. M. Morris, G. W. Kerr, and T. R. Ophel, Nucl. Phys. A112, 97 (1968).

[29]J. L. Fowler, Phys. Rev. 147, 870 (1966).

[30]H. L. Anderson, W. C. Davidson, M. Glicksman, and U. E. Kruse, Phys. Rev. 100, 279 (1955).

[31]H. P. Hermsen, Ph.D. dissertation, Hamburg, Germany, 1968 (unpublished).

[32]C. N. Davids, Nucl. Phys. 110, 619 (1968).

[33]S. R. Salisbury and H. T. Richards, Phys. Rev. 126, 2147 (1962).

[34]E. Baumgartner and P. Huber, Helv. Phys. Acta 26, 545 (1953).

[35]G. V. Gorlov, N. S. Lebedeva, and V. M. Morozov, Dokl. Akad. Nauk SSSR 158, 574 (1964) [transl.: Soviet Phys. – Doklady 9, 806 (1965)].

[36]W. P. Bucher, W. B. Beverly, G. C. Cobb, and F. L. Hereford, Phys. Rev. 115, 961 (1959).

[37]C. A. Kelsey, S. Kobayashi, and A. S. Mahajan, Nucl. Phys. 68, 413 (1965).

[38]B. E. Wenzel and M. F. Steuer, Phys. Rev. 137, B80 (1965).

[39]T. G. Miller and J. A. Biggerstaff, Nucl. Phys. A124, 637 (1969).

[40]J. T. Reynolds, C. J. Slavik, C. R. Lubitz, and N. C. Francis, Phys. Rev. 176, 1213 (1968).

[41]R. B. Schwartz, H. T. Heaton, III, and R. A. Schrack, Bull. Am. Phys. Soc. 15, 567 (1970); R. B. Schwartz, private communication.

[42]P. Stoler, J. C. Clement, C. G. Goulding, R. C. Block, and P. F. Yergin, Bull. Am. Phys. Soc. 15, 1668 (1970).

[43]J. B. Marion and J. L. Fowler, in *Fast Neutron Physics Part II* (see Ref. 18), p. 1413.

[44]R. O. Lane, A. S. Langsdorf, Jr., J. E. Monahan, and A. J. Elwyn, Ann. Phys. (N.Y.) 12, 135 (1961).

[45]A. J. Elwyn and R. O. Lane, Nucl. Phys. 31, 78 (1962).

[46]P. S. Dubbeldam, C. C. Jonker, and H. J. Boersma, Nucl. Phys. 15, 452 (1960).

[47]P. J. Pasma, Nucl. Phys. 6, 141 (1958).

[48]H. B. Willard, J. K. Bair, and J. D. Kington, Phys. Rev. 98, 669 (1955).

[49]D. G. Fleming, J. Cerny, C. C. Maples, and N. K.

Glendenning, Phys, Rev. 166, 1012 (1968).
[50]W. Galati, J. D. Brandenberger, A. Obst, and J. L. Weil, Bull. Am. Phys. Soc. 13, 1388 (1968)
[51]G. Wittwer, H. G. Clerc, and G. A. Beer, Phys. Letters 30B, 634 (1969).
[52]D. B. James, G. A. Jones, and D. H. Wilkinson, Phil. Mag. 1, 949 (1956).

PHYSICAL REVIEW C VOLUME 5, NUMBER 5 MAY 1972

Tests for T Invariance in Allowed Nuclear Beta Decay

Barry R. Holstein*
Department of Physics and Astronomy, University of Massachusetts, Amherst, Massachusetts 01002
(Received 5 January 1972)

Various tests of T invariance involving allowed nuclear β decays are discussed. T-violating correlations are calculated to first order in recoil terms E/M and electromagnetic final-state scattering corrections are given.

I. INTRODUCTION

Since the discovery of CP violation by Christenson, Cronin, Fitch, and Turlay[1] many experiments have been done seeking the resultant T violation predicted by the CPT theorem.[2] Some of the most sensitive tests have been provided by searches for a correlation of the form $J \cdot p_e \times p_\nu$ in the β decay of Ne^{19} by Calaprice *et al.*[3] and the measurements, utilizing the Mössbauer effect, of the angular correlation of linearly polarized photons with nuclear orientation (i.e., a correlation of the form $J \cdot e_\gamma J \cdot k_\gamma J \cdot e_\gamma \times k_\gamma$) by Blume and Kistner[4] and by Atac *et al.*[5] The former seeks T violation in the weak interaction, while the latter experiments are sensitive to electromagnetic T nonconservation. In both cases the results are thus far negative.[6]

We consider in this note the possibility of observing T violation in nuclear β decay. Section II reviews the suggestion by Kim and Primakoff[7] that experiments on Ne^{19} alone may not answer the question as to whether the weak interaction is T invariant inasmuch as, being an analog decay, it is not able to reveal the presence of a T-violating second-class current.[8] Also, more general T-nonconserving correlations in allowed nuclear β decay are discussed.

In Sec. III the electromagnetic scattering correlations are given, as calculated for specific transitions by Callan and Treiman,[9] by Chen,[10] and by Brodine,[11] and the contribution of the induced tensor is included.

Finally, in Sec. IV we study the feasibility of seeking T violation in a β-γ process, wherein the need for experimental detection of the small nuclear recoil is obviated.[12] A general expression for such correlations and the electromagnetic scattering corrections are given.

II. T VIOLATION IN ALLOWED NUCLEAR β DECAY

β-decay experiments which might reveal possible time-reversal violation were suggested by Jackson, Treiman, and Wyld in 1957.[13] They pointed out that measurement of the correlation $J \cdot p_e \times p_\nu$,

$$\frac{d^5\Gamma}{dE d\Omega_{\hat{e}} d\Omega_{\hat{\nu}}} \propto \left(1 + D\frac{\vec{J}}{J} \cdot \frac{\vec{p}_e \times \vec{p}_\nu}{E_e E_\nu} + \cdots\right),$$

was sensitive to the relative phase between the Fermi and Gamow-Teller matrix elements

$$D = \pm \frac{2\,\mathrm{Im} g_V M_F g_A^* M_{GT}^*}{g_V^2 |M_F|^2 + g_A^2 |M_{GT}|^2} \left(\frac{J}{J+1}\right)^{1/2}, \tag{1}$$

where M_F (M_{GT}) is the Fermi (Gamow-Teller) matrix element for the transition being studied, J is the spin of the parent nucleus, and the upper (lower) sign refers to electron (positron) decay.

Since then experiments measuring D have utilized neutron β decay[14] and $Ne^{19} \to F^{19} + e^+ + \nu_e$,[3] but no T violation has been found. Kim and Primakoff pointed out, however, that such experiments are primarily sensitive to the phase difference between M_F, M_{GT} so that when parent and daughter states are isotopic analogs, as is the case for the two decays which have been studied, only first-class currents can contribute and no limits are placed on second-class T-violating currents.

In order to examine this situation more carefully, we shall assume the validity of the usual current-current weak interaction and of the conserved-vector-current (CVC) hypothesis.[15] Then the β-decay amplitude is given by (for electron-decay; modifications appropriate to positron de-